[AMERICAN JOURNAL OF SCIENCE, VOL. 296, APRIL, 1996, P. 333–393]

American Journal of Science

APRIL 1996

DEHYDRATION, PARTIAL MELTING, AND ASSIMILATION OF METABASALTIC XENOLITHS IN GABBROS OF THE KAP EDVARD HOLM COMPLEX, EAST GREENLAND

MARK E. BRANDRISS*, DENNIS K. BIRD**, JAMES R. O'NEIL***, and ROBERT L. CULLERS****

ABSTRACT. Partially assimilated xenoliths of metabasaltic lava are locally abundant in Eocene gabbros of the Kap Edvard Holm Complex in East Greenland. The xenoliths range from centimeters to >100 m in length and consist mainly of hornfelsic augite, orthopyroxene, plagioclase, olivine, magnetite, and ilmenite, with two-pyroxene equilibration temperatures of ~1050°C. The hornfelses have been strongly depleted in incompatible elements due to extraction of an anatectic liquid. Melt fractions of roughly 30 to 50 percent are estimated from trace element modeling. Devolatilization or dehydration-melting of xenoliths released hydrous liquids into the gabbroic magma, locally causing replacement of gabbroic cumulates by bodies of peridotite and coarse-grained to pegmatitic gabbro.

The xenoliths contain hornfelsic minerals with $\delta^{18}O$ values as low as −5.5 permil. The low-$\delta^{18}O$ values were inherited from the country rock protoliths, which had previously been altered by low-$\delta^{18}O$ hydrothermal fluids of meteoric origin. Oxygen isotope fractionations between plagioclase and pyroxene are close to equilibrium values for magmatic temperatures, indicating that the xenoliths recrystallized in isotopic equilibrium during heating and subsequently underwent little or no oxygen isotope exchange during subsolidus cooling and alteration of the pluton.

Many xenoliths contain igneous bodies that crystallized from trapped partial melts. These include pegmatitic pods consisting of hornblende, andesine, apatite and phlogopite, and plagioclase-rich leucosomes in which pockets of hornblende-rich pegmatite are locally developed. The abundance of hydrous minerals in these melt bodies suggests that melting was facilitated by the presence of H_2O in the hydrothermally altered metabasaltic protoliths. Alteration and hydra-

* Department of Geological and Environmental Sciences, Stanford University, Stanford, California 94305-2115, Present address: Department of Geological Sciences, 2534 C.C. Little Building, 425 E. University Ave., University of Michigan, Ann Arbor, Michigan 48109-1063.

** Department of Geological and Environmental Sciences, Stanford University, Stanford, California 94305-2115.

*** Department of Geological Sciences, 2534 C.C. Little Building, 425 E. University Ave., University of Michigan, Ann Arbor, Michigan 48109-1063.

****Department of Geology, Thompson Hall, Kansas State University, Manhattan, Kansas 66506.

tion of the country rock metabasalts thus enhanced the potential for contamination of magmas with hydrous fluids and partial melts.

INTRODUCTION

Mafic crustal xenoliths are abundant in gabbroic plutons in a variety of tectonic settings. Such xenoliths are commonly refractory and thus difficult to melt and assimilate. The potential for petrologically significant contamination of magmas by mafic xenoliths can, however, be greatly enhanced if the xenoliths are hydrous. Devolatilization of xenoliths is potentially an efficient means of contaminating magmas with H_2O, because volatiles released from xenoliths, unlike those contained in wall rocks, must be absorbed by the intruding magma (Taylor and Sheppard, 1986). In addition, because H_2O lowers solidus temperatures dramatically, its presence in mafic xenoliths can facilitate melting and thus increase the amounts of melt assimilated (Clemens and Vielzeuf, 1987).

These factors suggest that contamination of magmas by mafic xenoliths will occur most readily in regions of extensive plutonic-hydrothermal activity, where vast amounts of rock become hydrated during reaction with meteoric or seawater-derived fluids. One example is Iceland, where chemical features of many basaltic lavas reflect contamination by hydrothermally altered mafic crust (Hattori and Muehlenbachs, 1982; Steinthorsson and others, 1987; Sigmarsson, Condomines, and Fourcade, 1992). Other examples include ophiolitic plutons, in which assimilation of altered mafic xenoliths is a common process (Stakes, Taylor, and Fisher, 1984; Pedersen, 1986; Malpas, Brace, and Dunsworth, 1989; Bédard and Hébert, 1992). Partial melting or devolatilization of hydrated metabasic xenoliths has also been documented in oceanic gabbros of the Southwest Indian Ridge (Stakes, 1991; Stakes and others, 1991), in synorogenic gabbros of the Fongen-Hyllingen intrusion (Wilson and Larsen, 1985; Habekost and Wilson, 1989) and in rift-related gabbros of the North Atlantic Tertiary Igneous Province (Taylor and Forester, 1979; Bird, Manning, and Rose, 1988; Rose, 1989; Brandriss, 1993).

The subject of this study is the Kap Edvard Holm intrusive complex, part of an early Tertiary plutonic center on the east coast of Greenland (fig. 1). Gabbros of the complex locally contain hornfelsed and dehydrated xenoliths of hydrothermally altered basaltic lava. Most of these xenoliths underwent partial melting, yielding anatectic liquids that were in some cases trapped in the hornfelsed residua (fig. 2). These xenoliths provide an excellent opportunity to investigate processes of dehydration, partial melting and assimilation of hydrothermally altered mafic rocks in a gabbroic pluton.

GEOLOGIC SETTING

Kap Edvard Holm Complex

The Kap Edvard Holm Complex consists mainly of Eocene layered gabbros intruded locally by mafic dikes and syenitic plutons (fig. 3). The

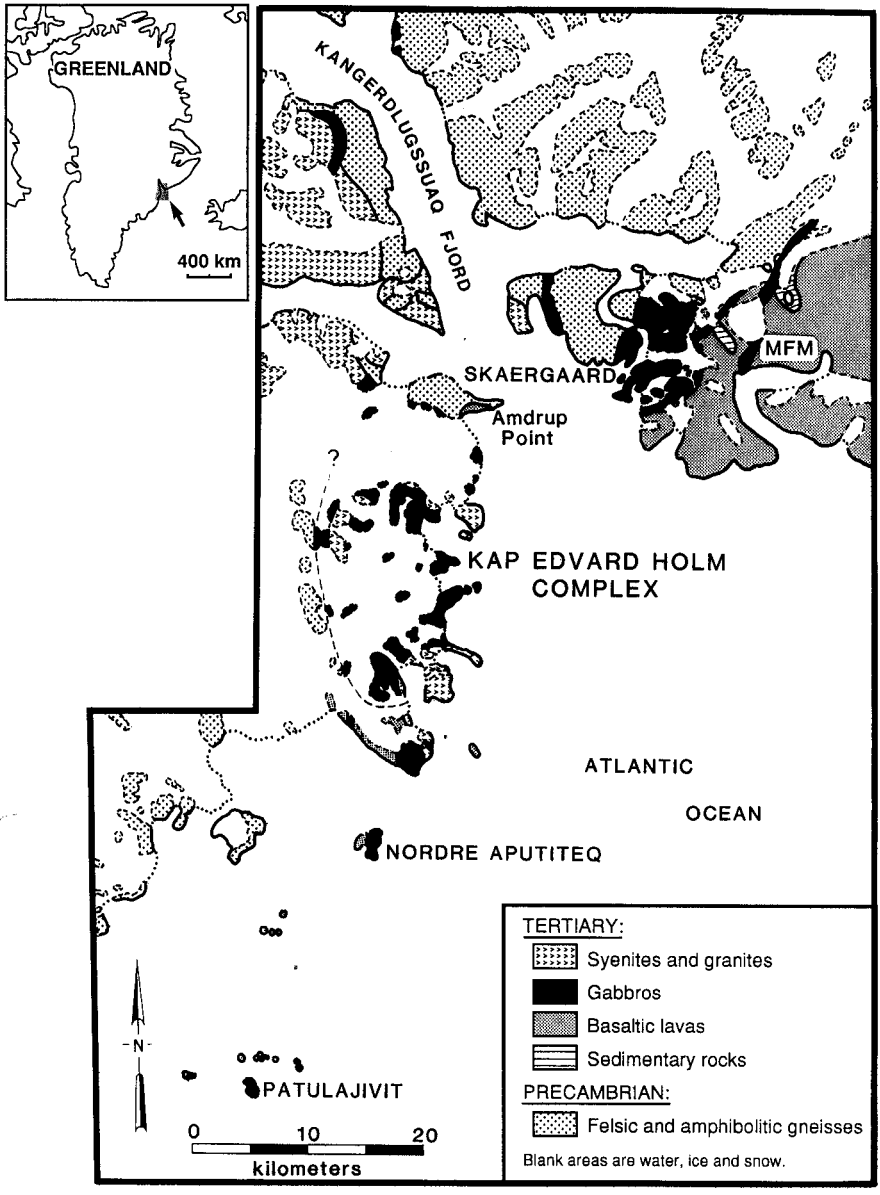

Fig. 1. The Kap Edvard Holm Complex and surrounding area. MFM = Miki Fjord Macrodike.

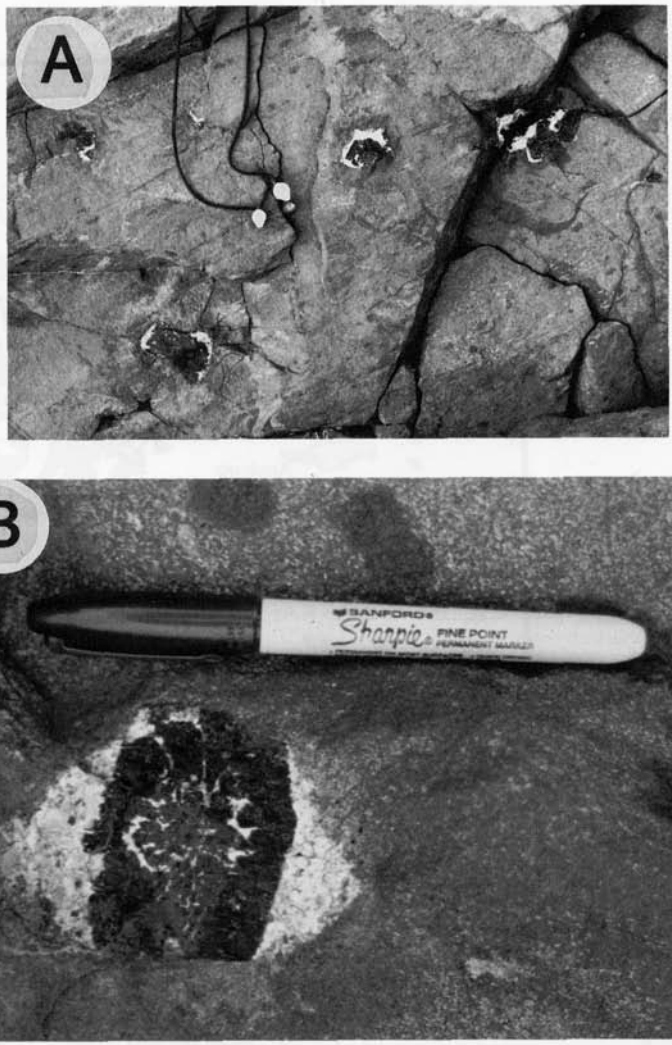

Fig. 2. Pegmatitic pods that crystallized from partial melts trapped in xenoliths. (A) Swarm of pegmatitic pods (black and white patches) in a hornfelsed metabasaltic xenolith. Two hand lenses on a string for scale. (B) Close-up of a pegmatitic pod in xenolith hornfels. The dark mineral is hornblende, the light minerals are andesine and apatite.

layered gabbros have a stratigraphic thickness exceeding 5000 m and consist mostly of plagioclase + augite ± olivine ± titanomagnetite ± ilmenite mesocumulates (Deer and Abbott, 1965; Wager and Brown, 1967; Elsdon, 1969, 1971; Abbott and Deer, 1972; Bernstein and others, 1992). These formed in a magma chamber episodically replenished by

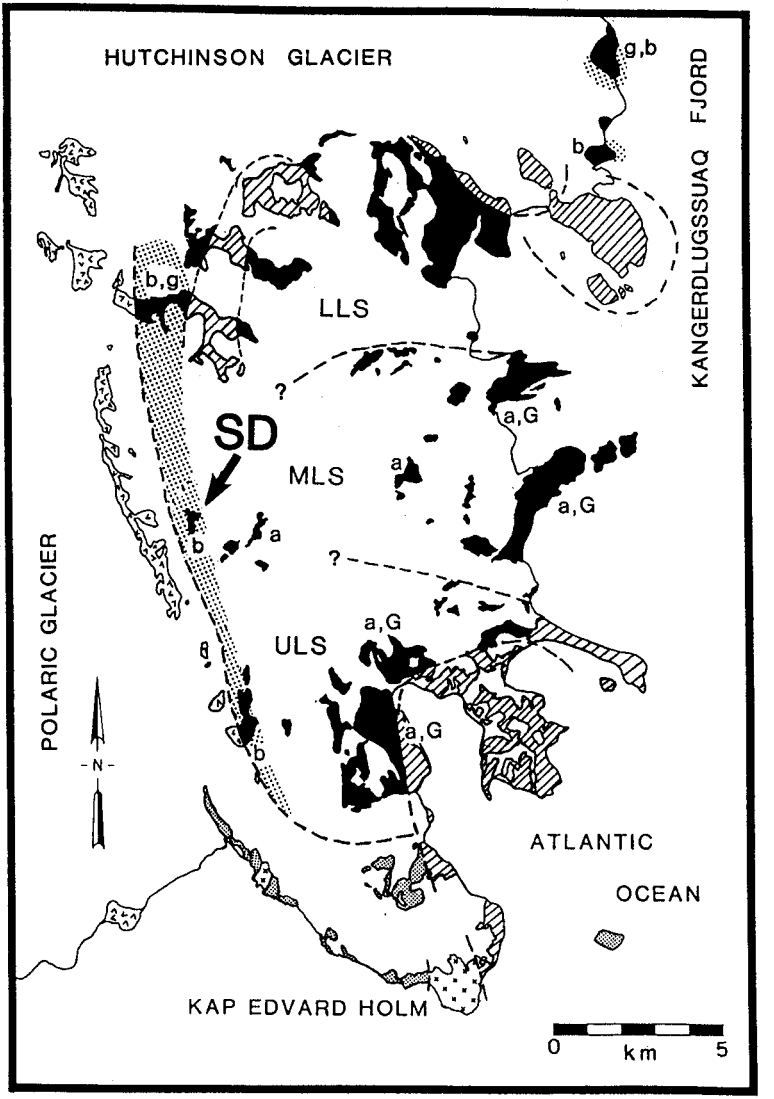

KAP EDVARD HOLM COMPLEX:

- Gabbros and mafic dike swarms
- Syenites, syenite breccias, and gabbro-syenite hybrid rocks
- Zones containing metabasalt xenoliths

Xenoliths: b = basalt, g = gneiss, a = anorthosite, G = gabbro

OTHER TERTIARY ROCKS:

- Gabbroic intrusions
- Lower Basalt lavas

PRECAMBRIAN ROCKS:

- Felsic and amphibolitic gneisses

Fig. 3. Geologic map of the Kap Edvard Holm Complex, showing the distribution of xenoliths and the location of the study area (SD = Stand and Deliver Nunatak). LLS, MLS, and ULS are Lower, Middle, and Upper Layered Series (after Abbott and Deer, 1972).

injections of basaltic magma (Bernstein and others, 1992; Tegner, Wilson, and Brooks, 1993). Along its western contact the gabbro complex is bordered by a narrow zone of fine-grained mafic hornfels, interpreted to be a metamorphosed remnant of the earliest phase of intrusion (Elsdon, 1969; Abbott and Deer, 1972).

The gabbros are hosted by Precambrian gneisses, Paleocene flood basalts, and volumetrically minor amounts of Cretaceous and Paleocene sedimentary rocks (fig. 1). The basalts form a lava pile up to 5 km thick which accumulated unconformably on the gneisses immediately prior to the onset of Tertiary oceanic rifting (Wager, 1947; Soper and others, 1976; Nielsen and others, 1981; Nielsen and Brooks, 1981; Brooks and Nielsen, 1982a,b; Bott, 1987; Noble, Macintyre, and Brown, 1988). Contacts between the gabbros and basaltic lavas are not exposed, but stratigraphic projections indicate that the lavas host the complex to the east and south and probably formed the roof of the intrusion prior to erosion. Layered gabbros near the margins of the complex contain abundant xenoliths of basaltic lava (figs 3 and 4A).

Basaltic Country Rocks

The xenoliths were derived from a 1.5 km-thick volcanic unit known as the Lower Basalts, which consist of lava flows, hyaloclastites, breccias, and tuffaceous sediments of the Vandfaldsdalen and Miki Formations (Nielsen and others, 1981). Lava compositions range from picrite to tholeiitic andesite (table 1) with olivine tholeiite being the most common type (Brooks, Nielsen, and Petersen, 1976; Nielsen and others, 1981; Gill and others, 1988; Holm, 1988).

The Lower Basalts have been regionally metamorphosed to subgreenschist and greenschist assemblages containing combinations of chlorite, epidote, prehnite, albite, quartz, titanite, zeolites, microcline, and calcite (Bird and others, 1985; Manning and Bird, 1995). These regional parageneses have been overprinted by contact metamorphism near plutons, dikes, and sills (Taylor and Forester, 1979; Bird and others, 1985; Manning and Bird, 1991, 1995; Manning, Ingebritsen, and Bird, 1993). Grades as high as the sanidinite facies were reached in the aureoles of large plutons such as the Skaergaard intrusion (Manning and Bird, 1991, 1995).

During metamorphism the basalts were infiltrated by low-$\delta^{18}O$ hydrothermal fluids of meteoric origin. These fluids exchanged oxygen with the rocks and depleted them in ^{18}O (Taylor and Forester, 1979; Bird, Manning, and Rose, 1988; Manning and Bird, 1995). Measured whole-rock $\delta^{18}O$ values range from -2.3 to $+4.1$ permil, substantially lower than typical values of fresh mantle-derived basalts worldwide ($+5$ to $+7$ permil; Kyser, 1986).

Abundances of secondary minerals are variable at the outcrop scale. In porous zones, such as breccias and the vesiculated bases and tops of lava flows (Bird and others, 1985; Manning and Bird, 1991, 1995),

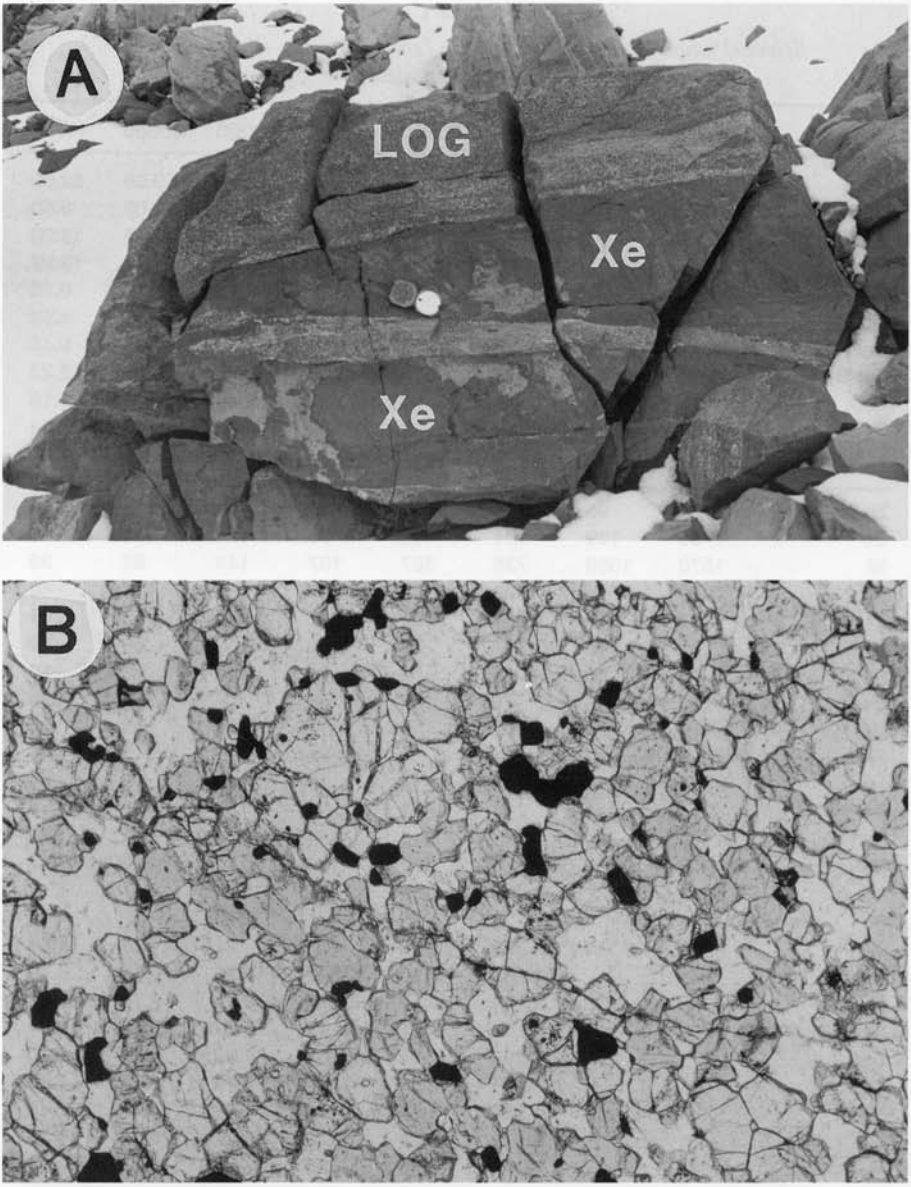

Fig. 4. (A) Parts of two metabasaltic xenoliths (Xe) in layered olivine gabbro (LOG), with a Brunton compass for scale. These xenoliths are smaller than most, but the lenticular shapes are typical of xenoliths of all sizes. (B) Thin section of a hornfelsed mafic xenolith (KEH408). Field of view is 3 mm wide.

TABLE 1

Selected whole-rock analyses of the Lower Basalts, illustrating the range of compositions

Sample	40651	40032	20332	20351	1133	40020	40630	40632
SiO_2	44.92	46.52	48.56	49.69	48.70	52.79	50.66	52.50
TiO_2	1.17	2.81	2.19	2.77	2.34	1.92	4.09	3.50
Al_2O_3	5.56	6.05	11.06	8.21	12.59	13.79	12.62	13.09
Fe_2O_3*	12.71	13.81	14.29	14.53	12.72	10.87	14.61	13.27
MnO	0.21	0.21	0.17	0.17	0.17	0.15	0.18	0.18
MgO	29.60	20.30	12.20	11.40	8.14	7.33	5.80	4.59
CaO	5.55	9.07	9.74	11.13	11.47	8.58	7.33	9.45
Na_2O	0.14	1.48	2.06	1.53	2.02	4.89	3.00	2.23
K_2O	0.12	0.28	0.39	0.39	0.31	0.03	2.11	1.16
P_2O_5	0.19	0.23	0.32	0.28	0.20	0.20	0.26	0.34
Total	100.17	100.76	100.98	100.10	98.66	100.55	100.66	100.31
Zn	98	95	125	108		95	123	119
Cu	55	190	104	82	75	104	104	66
Ni	1570	1099	735	387	137	143	88	39
Cr	1800	1748	1396	1057	367	365	115	44
V	158	239	285	360	342	278	445	364
Co	107	118	92	83	65	53	66	49
Sc	16	25	20	30	30	27	28	23
Ba	39	144	70	134	87	7	718	334
Rb	4	9	5	6	3		49	25
Th	2	7	1	2	1	1	2	5
Nb	4	14	9	14	10	8	19	18
Ta		1	1	1	1	1	1	1
Sr	89	319	250	218	324	365	847	567
Zr	50	130	130	170	144	143	206	248
Hf			4	5	2	4	7	6
Pb			1	2		2	2	6
Ga	9	14	21	18		21	20	24
La			10.04	17.30	9.30	12.56	25.25	28.73
Ce			27.71	49.29	22.70	33.28	59.18	71.83
Sm			5.60	7.15	4.64	5.24	8.13	9.34
Eu			1.68	2.08	1.51	1.63	2.57	2.80
Tb			0.87	0.99	0.71	0.78	1.13	1.28
Yb			2.00	1.77	1.66	1.66	1.65	2.49
Lu			0.27	0.20	0.28	0.27	0.24	0.30
Y	10	17	25	24	28	23	27	32

Oxides in wt%, elements in ppm.

SOURCES OF DATA: sample 1133 from Brandriss (1993) and Manning and Bird (1995); all others from Gill and others (1988, and unpublished data) and Holm (1988, and unpublished data).

* All Fe as Fe_2O_3.

cavities were filled with hydrous secondary minerals, and the localized availability of pore fluids facilitated alteration and hydration of the surrounding rock (Manning and Bird, 1995). Formation of pore-filling minerals resulted in substantial but localized changes in whole-rock composition. A study of sub-greenschist to sanidinite-grade Lower Basalts in the Skaergaard aureole has shown that, except in these porous zones, subsolidus alteration had little effect on whole-rock compositions other than producing changes in isotopic ratios and volatile concentrations (Manning and Bird, 1995).

The Lower Basalts near the Kap Edvard Holm Complex are similar to those already described. Lavas on Amdrup Point (fig. 1) resemble the actinolite-chlorite zone Lower Basalts described by Manning and Bird (1995) and have been similarly depleted in deuterium and ^{18}O ($\delta D = -136$ permil and $\delta^{18}O = +3.2$ permil for a massive flow; Brandriss, 1993). Metabasalts exposed to the south of the complex appear to be typical Miki Formation flows of the Lower Basalts (T.F.D. Nielsen, personal communication).

GEOLOGY OF THE STUDY AREA

The study area is a group of cliffs containing abundant xenoliths of metabasalt. These cliffs, located near the western contact of the intrusion (fig. 1), are referred to collectively as "Stand and Deliver Nunatak" (fig. 5).

Layered Gabbros

Modally layered, laminated gabbros constitute ~80 percent of the outcrop at Stand and Deliver Nunatak. The layering is typically very faint (fig. 4A) except in a few stratigraphic intervals where decimeter to meter-scale layers of melanocratic rock ("mafic macrolayers") are developed. Primary minerals in the gabbro are plagioclase, clinopyroxene, olivine, titanomagnetite, ilmenite, and trace amounts of intergranular hornblende and orthopyroxene.

Metabasaltic Xenoliths

Fine-grained metabasaltic xenoliths constitute roughly 10 percent of the outcrop. They are lenticular or tabular, lie concordant to layering, and range from centimeters to >100 m in length and up to 5 m in thickness. Large xenoliths (> 10 m) constitute by far the greatest portion of the xenolithic mass.

The xenoliths consist mainly of anhydrous granoblastic hornfels composed of clinopyroxene + plagioclase + titanomagnetite ± orthopyroxene ± olivine ± ilmenite (fig. 4B). Many also contain discrete bodies with igneous textures, including pods of hornblende-phlogopite pegmatite (fig. 2), bands of medium-grained gabbro (fig. 6), and plagioclase-rich leucosomes in which pegmatitic zones are locally developed (fig. 7).

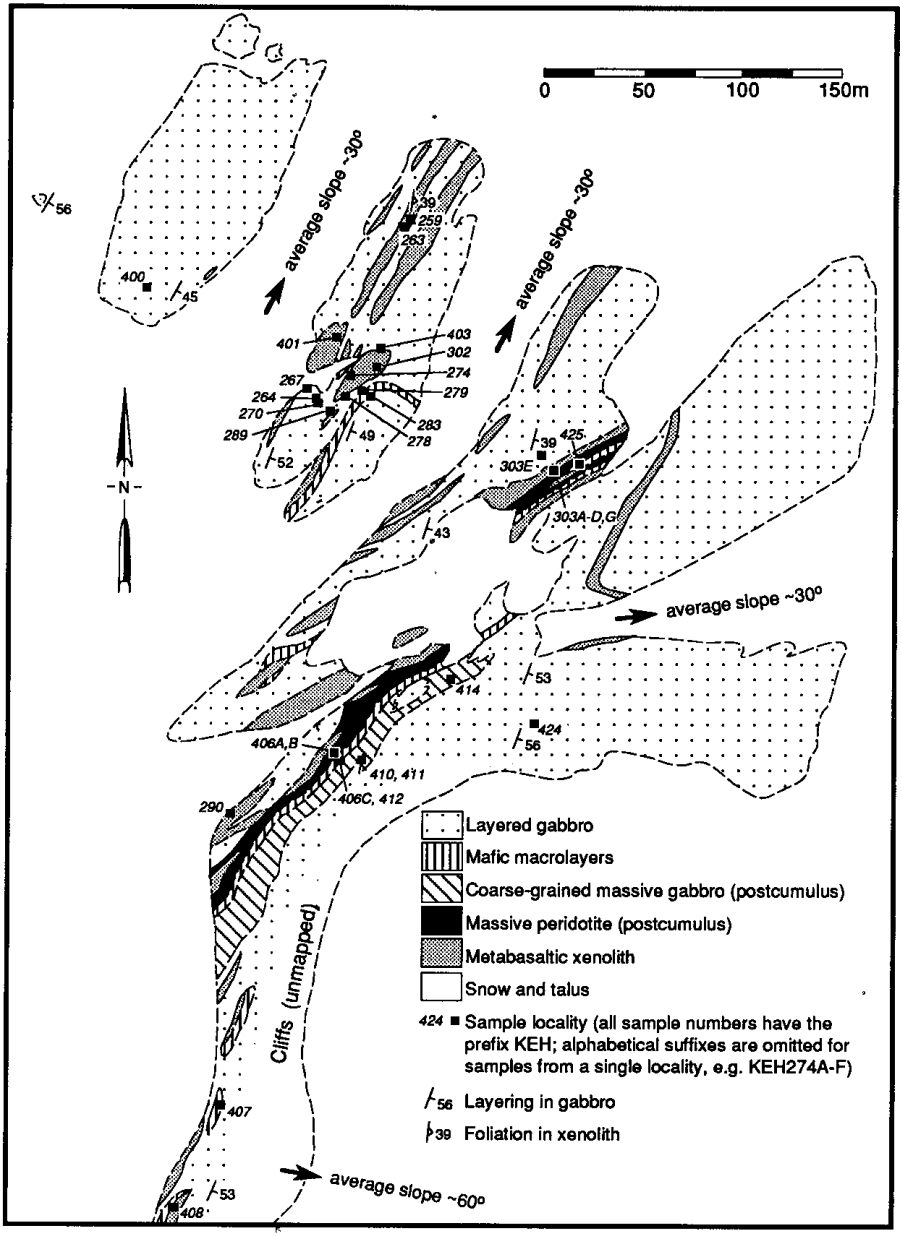

Fig. 5. Geologic map of Stand and Deliver Nunatak.

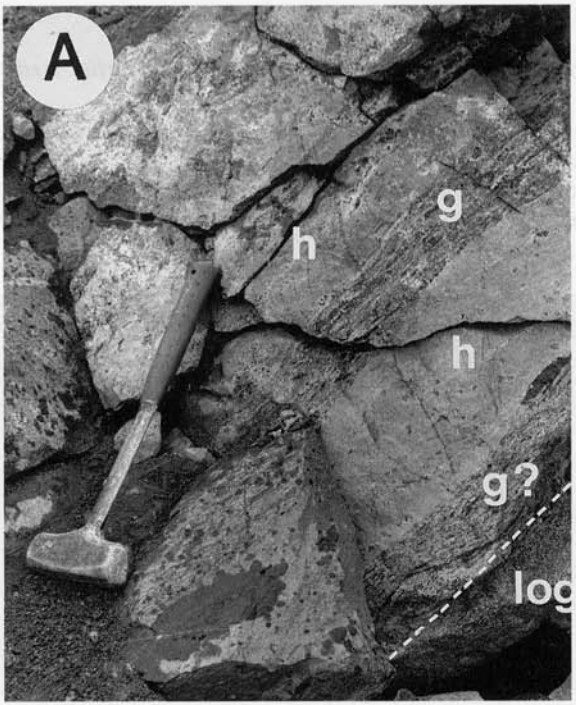

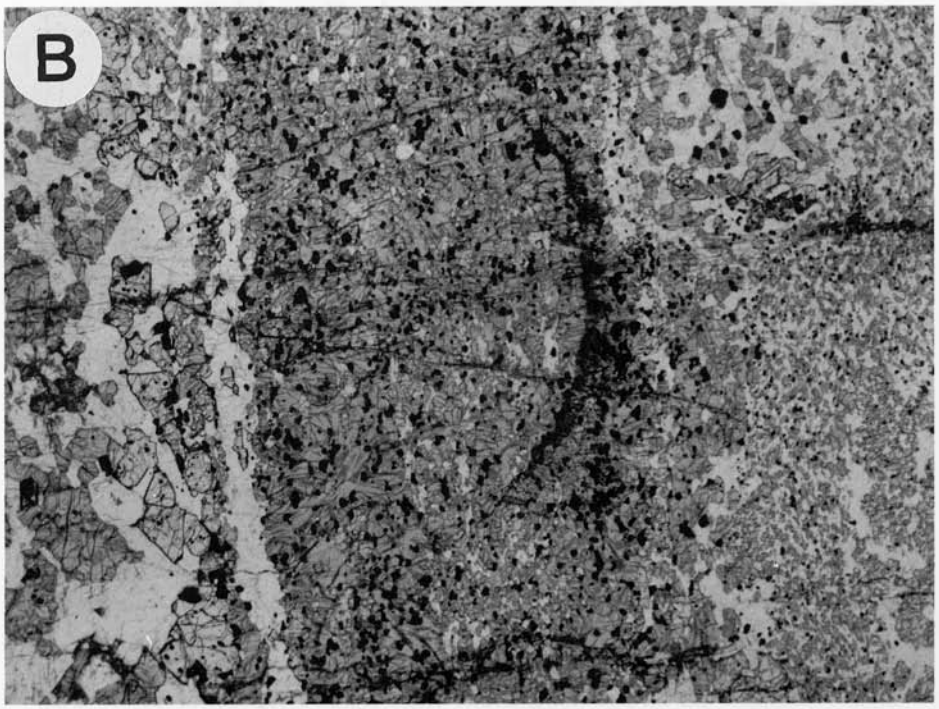

Fig. 6. (A) A band of gabbro (g) enclosed in granoblastic xenolith hornfels (h). Another band of gabbro, possibly also part of the xenolith (g?), is in contact with layered olivine gabbros of the intrusion (log) at lower right. The dark patch to the lower right of the hammer head is a wet spot. (B) Contact between the gabbroic band (left) and fine-grained hornfels (right), with a clinopyroxene-rich melanosome in-between. Field of view is 23 mm wide.

These bodies are enclosed in the hornfelses, suggesting that they formed from melts of the xenoliths themselves.

Many xenoliths contain relict volcanic structures such as hornfelsed amygdules and flow contacts (fig. 8). Such xenoliths are obviously frag-

Fig. 7. Leucosome (pale band at arrow) in a metabasaltic xenolith. The entire outcrop (excluding rubble) is part of a single xenolith. Note brecciation of the hornfels by the leucosome at upper right.

Fig. 8. Relict volcanic structures. The entire outcrop is part of a single xenolith containing a contact between two lava flows. The contact is slightly convex toward the upper left and is marked with an arrow; it truncates bands of pale amygdules to the left of the hammer. A leucosome follows the contact at upper right. Pale patches above and to the left of the arrow are plagioclase-hornblende pegmatite pods.

ments of basaltic lava. Others lack recognizable volcanic features, and some could conceivably be pieces of amphibolite from the Precambrian gneisses or gabbroic hornfels from the western contact zone. As discussed later, however, the chemical characteristics of the xenoliths generally support their identification as fragments of the Tertiary lavas.

Postcumulus Rocks

Near many xenoliths, the layered gabbros have been replaced locally by discordant bodies of peridotite and coarse-grained to pegmatitic gabbro. These comprise two distinct size populations: (1) small bodies, which form irregular stringers and pods ranging from centimeters to meters in length (fig. 9); (2) larger bodies, which form semi-conformable sheets up to a few meters thick and extending for hundreds of meters along strike (fig. 5). All these postcumulus bodies are conspicuously associated with xenoliths, the smaller bodies being found only within a few meters of xenoliths, and the larger bodies overlying or partially enveloping swarms of xenoliths. Because of this intriguing association, the postcumulus rocks will be described in some detail.

The small postcumulus bodies typically cluster within a few centimeters or decimeters of gabbro-xenolith contacts. Ultramafic and coarse-grained gabbroic bodies commonly occur together, forming a distinctly bimodal assemblage (fig. 9). The ultramafic rocks consist mainly of olivine and clinopyroxene with lesser magnetite, orthopyroxene, and plagioclase. The gabbroic rocks consist mainly of plagioclase, clinopyroxene, and magnetite, with olivine conspicuously absent. The ultramafic and gabbroic bodies also contain a few percent interstitial titanian hornblende or phlogopite, phases which are present in only trace amounts in the layered gabbros.

The small ultramafic bodies have sharp contacts and irregular or branching forms (fig. 10A). They are generally discordant but locally penetrate along planes of layering and lamination in the host gabbro (fig. 10B). Some ultramafic bodies are discontinuously zoned from olivine-rich cores to pyroxene-rich rims (fig. 10A), with the olivine-rich rocks containing plagioclase and pyroxene only as late interstitial phases. The gabbroic bodies typically occur as discordant pods or stringers or less commonly as rinds along xenolith surfaces (fig. 9). Their contacts with the layered gabbros range from sharp to gradational.

The larger postcumulus bodies outcrop in two stratigraphic zones, each of which contains prominent mafic macrolayers and abundant xenoliths (fig. 5). Each zone contains a massive peridotitic unit several meters thick and extending for tens or hundreds of meters along strike. In one zone the peridotitic rocks are overlain by several meters of massive, coarse-grained, olivine-free gabbro, producing a bimodal association of rock types similar to that found in the smaller postcumulus bodies. Although broadly conformable, the large gabbroic and peridotitic bodies locally crosscut the overlying layered gabbros and are therefore clearly of postcumulus origin. In one place, layering can be traced across

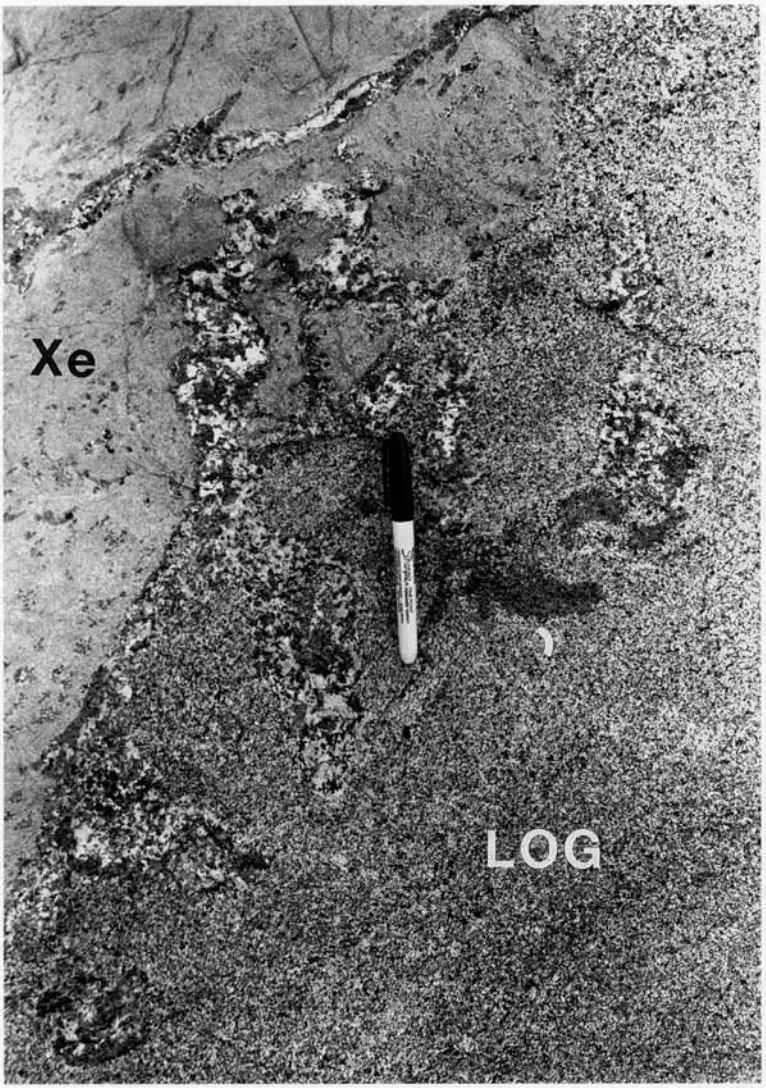

Fig. 9. Contact between a metabasalt xenolith (Xe) and faintly layered olivine gabbro (LOG). Coarse-grained gabbro forms pale irregular stringers along and near the contact, and irregular bodies of peridotite are visible to the right of the pen.

a discordant contact between layered gabbro and peridotite, implying a replacive rather than intrusive origin for the postcumulus rocks (fig. 11). Equilibration temperatures of 1020° to 1070°C for the peridotites have been calculated by two-pyroxene thermometry (Brandriss, ms). This implies formation under magmatic conditions.

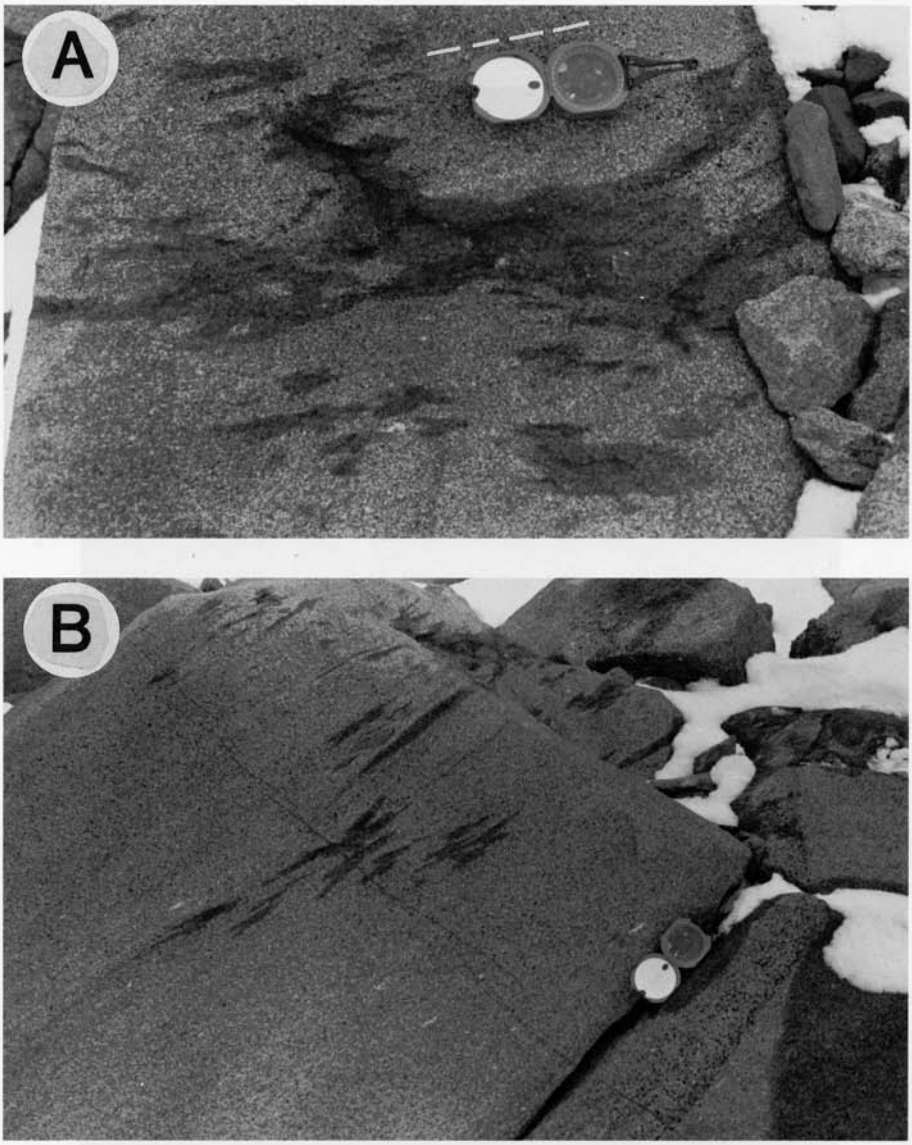

Fig. 10. Postcumulus ultramafic bodies cutting layered gabbro. (A) Branching peridotite bodies with olivine-rich cores. The cores weather deeply and, in the photograph, appear slightly darker than the rest of the peridotite (for example, to lower left of compass). The faint trend of layering is indicated by the dotted line. A swarm of xenoliths outcrops about 1 m below the photograph. (B) Outcrop surface perpendicular to the one in (A), showing peridotite bodies penetrating along planes of layering and lamination.

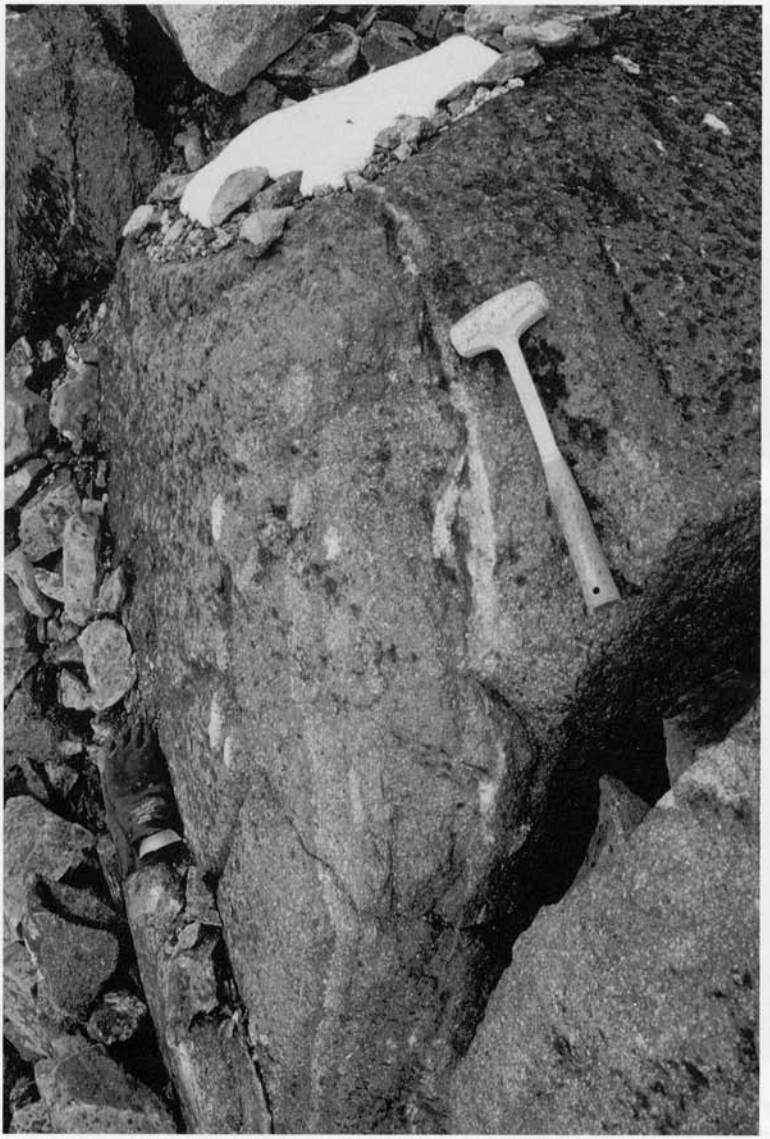

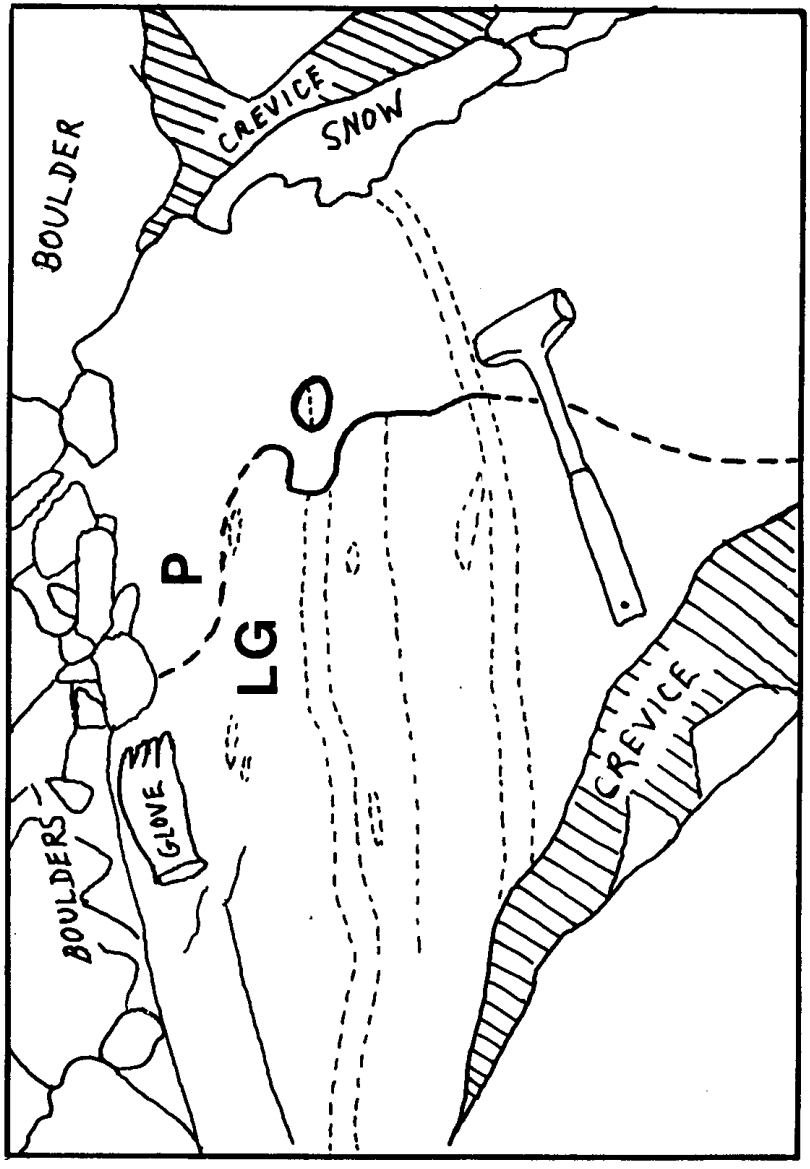

Fig. 11. Layered gabbro (at left) and discordant postcumulus peridotite. The peridotite is an apophyse from a semi-conformable peridotite body >75 m long. In the drawing, the contact is shown by the line separating layered gabbro (LG) from peridotite (P). The prominent leucocratic layer immediately above the hammer can be traced into the peridotite, but the less distinct layers above it have been truncated.

Brandriss (ms) proposed that the postcumulus bodies formed when partially solidified gabbroic cumulates were infiltrated by H_2O-rich fluids or melts released from the metabasaltic xenoliths. These hydrous liquids were inferred to have infiltrated the cumulates and resorbed plagioclase, leaving peridotitic residua; the plagioclase-rich liquids then segregated, mixed with nearby gabbroic cumulates, and crystallized as bodies of coarse-grained to pegmatitic gabbro. This hypothesis will be discussed further after the following examination of the xenoliths themselves.

METABASALTIC XENOLITHS

Because the Lower Basalts have been studied in some detail, the xenoliths provide an excellent opportunity to compare hornfelsed and partially melted xenoliths with their inferred metabasaltic protoliths. A detailed examination of the xenoliths is presented in this section.

Analytical Methods

Nine metabasaltic xenoliths from Stand and Deliver Nunatak were subjected to chemical and isotopic analysis, including one that was sampled from rim to core (samples KEH274A-F). These xenoliths are described in table 2.

Samples of texturally homogeneous hornfels were crushed and powdered for whole-rock chemical analysis of major and trace elements by X-ray fluorescence spectrometry. Analyses were performed at Stanford University, using a fused disk method based on the technique of Norrish and Hutton (1969) for major elements and a pressed powder method based on the technique of Norrish and Chappell (1977) for trace elements. Some samples were also analyzed for selected trace elements (including REE) by instrumental neutron activation analysis at Kansas State University, using methods adapted from Gordon and others (1968) and Jacobs and others (1977); the accuracy of these methods has been reported in Cullers and others (1979). Strontium isotope ratios of selected samples were measured at Rice University using standard chemical and spectrometric techniques. Oxygen isotope analyses of mineral separates were made at the University of Michigan, using a conventional BrF_5 extraction method similar to that of Clayton and Mayeda (1963). Compositions of minerals were determined by wavelength-dispersive electron microprobe analysis at Stanford University, using natural and synthetic oxide and silicate standards. Further analytical details are given in the appropriate tables of data and in Brandriss (ms).

Conditions of Xenolith Metamorphism

Pressure.—The study area is near the base of the Lower Basalts, where maximum pressures of ~2 kb were attained during thickening of the basalt pile (Nielsen and Brooks, 1981; Rosing and Lesher, 1992). This is taken as the upper limit for pressure at the time of stoping. The actual pressure may have been lower if the basalts were denuded prior to pluton emplacement.

Temperature.—Recrystallization temperatures for xenoliths were calculated using the two-pyroxene geothermometer of Davidson and Lindsley (1989) in the form presented by Andersen, Lindsley, and Davidson (1993). Pyroxene analyses are reported in tables 3 and 4. An independent calculation of temperature was made from each analysis, with consistency of the results providing a check for equilibrium between the two phases (Andersen, Lindsley, and Davidson, 1993). Results are summarized in table 5.

The average temperatures calculated for six samples from three xenoliths ranged from 1035 to 1073°C. There was good agreement between temperatures calculated independently from orthopyroxene and clinopyroxene in each sample (errors due to uncertainties in the electron microprobe analyses were roughly ±20°C for clinopyroxene and ±15°C for orthopyroxene). Calculated temperatures thus were similar for all three xenoliths analyzed, and a traverse through a 4-m-thick xenolith (samples KEH274B, D, F) recorded no significant difference between center and margin. The roughly equivalent results for all samples reflect either:

1. heating to approximately the same maximum temperature, which was somewhere between ~1000 and ~1100°C; or,
2. heating to some higher temperature, followed by diffusional re-equilibration during cooling with a closure temperature of 1000° to 1100°C.

In the latter case, subsolidus re-equilibration may have obliterated evidence for gradients in peak metamorphic temperature. In either case, temperatures approached or exceeded the solidi of dry and hydrous basalts (Yoder and Tilley, 1962; Holloway and Burnham, 1972; Helz, 1976; Spulber and Rutherford, 1983; Beard and Lofgren, 1991; Sisson and Grove, 1993).

Strontium Isotopes

Strontium isotope analyses of the xenoliths and host gabbro are presented in table 6. The xenoliths have $^{87}Sr/^{86}Sr$ values ranging from 0.7034 to 0.7046, indicative of derivation from the Tertiary basalts (0.7031-0.7094; Holm, 1988) rather than from the more radiogenic Precambrian amphibolites (Pankhurst, Beckinsale, and Brooks, 1976; Kays, Goles, and Grover, 1989; Stewart and DePaolo, 1990). The lowest values (<0.704) are similar to those of flows from the Miki Formation of the Lower Basalts (Fram, 1994) but are significantly lower than those of the host gabbro, thus supporting the assertion that the xenoliths are fragments of lava rather than cognate xenoliths from the chilled marginal zone of the pluton itself.

Oxygen Isotopes

Oxygen isotope analyses of minerals from the xenoliths and plutonic rocks are reported in tables 7 and 8. The $\delta^{18}O$ values of plagioclase are plotted against those of coexisting pyroxene in figure 12. All samples

TABLE 2

Metabasaltic xenoliths analyzed in this study

Description (xenolith dimensions in parentheses)		*Meters from xenolith margin*	*Mineralogy* (trace phases in parentheses)*
FOLIATED HORNFELSIC XENOLITH WITH LEUCOSOMES AND HORNBLENDE AUGEN (5m x >100m)			
KEH259A	Granoblastic hornfels with hb augen and small gabbroic stringers; 10 cm below prominent leucosome	0.35	cpx, opx, plag, mag, ilm
KEH259D	Leucosome, 8 cm thick; fine-grained granoblastic, with large (3mm) anhedral crystals of plag, cpx	0.20	plag, cpx, OX (opx, hb)
KEH259E	Margin of same leucosome as KEH259D, with pegmatitic zone and adjacent hornfels	0.25	fine-grained zone: plag, cpx, OX (opx, hb) pegmatitic zone: cpx, hb, plag, OX adjacent hornfels: cpx, OX, opx, plag
KEH263	Same leucosome as KEH259D, sampled 5 m away; fine-grained granoblastic with pegmatitic patches	~0.3	fined-grained zone: plag, cpx, OX (opx, hb) pegmatitic zone: cpx, hb, plag, OX
HORNFELSIC XENOLITH (0.2m x 1.1m)			
KEH267A	Granoblastic hornfels, with coarse stringers of cpx, ol	0.10	cpx, plag, ol, mag
HORNFELSIC XENOLITH WITH PEGMATITIC PODS (4m x 40m)			
KEH274A	Granoblastic hornfels, in contact with host gabbro	0 - 0.02	cpx, plag, ol, mag
KEH274B	Granoblastic hornfels, with trace poikilitic hb	0.3	cpx, plag, opx, ol, ilm, mag (hb)
KEH274C	Granoblastic hornfels, with traces of poikilitic hb, ap and intergranular phlog	0.9	cpx, plag, opx, ol, ilm, mag (hb, ap, phlog)
KEH274D	Granoblastic hornfels, with trace poikilitic hb, ap	1.8	cpx, plag, opx, ilm, mag (hb, ap)
KEH274E	Pegmatitic pod (~5 cm)	0.6	hb, plag, ap, phlog
KEH274F	Pegmatitic pod (~15 cm) and adjacent granoblastic hornfels	0.8	pegmatitic pod: hb, plag, ap, phlog (ilm, hornfels: plag, opx, cpx, ilm, mag (hb, ap)
KEH302	Pegmatitic pod (~10 cm)	~2	phlog, hb, plag, ap

HORNFELSIC XENOLITH WITH PEGMATITIC PODS (> a few meters)			
KEH290	Pegmatitic pod (~15cm) with adjacent granoblastic hornfels	?	pegmatitic pod: hb, phlog, plag, ap, OX (zr) hornfels: plag, opx, cpx, OX, ol
HORNFELSIC XENOLITH WITH GABBROIC BANDS (~1.5m x >80m)			
KEH303B	Granoblastic hornfels, with gabbroic band bordered by melanosome	0.20 - 0.25	hornfels: plag, cpx, ol, OX gabbroic band: plag, cpx, ol, OX melanosome: cpx, OX, ol, plag (opx)
KEH303G	Granoblastic hornfels, with roughly 10% small (2-3 cm) gabbroic stringers	~0.3	hornfels: cpx, plag, ol, OX gabbroic stringers: ol, plag, cpx, OX (hb)
HORNFELSIC XENOLITH (0.15m x 1.9m)			
KEH303F	Granoblastic hornfels	0 - 0.04	plag, cpx, OX, ol
HORNFELSIC XENOLITH (1.3m x 25m)			
KEH401	Granoblastic hornfels, with coarse orthopyroxene-rich zones	0.5	opx, plag, OX, cpx
HORNFELSIC XENOLITH (0.65m x >3m)			
KEH406A	Granoblastic hornfels with trace intergranular hb; in contact with postcumulus peridotite body	0 - 0.04	plag, cpx, OX, ol (hb)
HORNFELSIC XENOLITH (>1m x >10m)			
KEH408	Granoblastic hornfels with trace intergranular hb	>0.5	plag, ol, cpx, OX, opx (hb)

* plag = plagioclase, cpx = clinopyroxene, opx = orthopyroxene, ol = olivine, ilm = ilmenite, mag = magnetite, hb = hornblende, phlog = phlogopite, ap = apatite, zr = zircon, OX = magnetite +/− ilmenite

TABLE 3

Electron microprobe analyses of hornfelsic clinopyroxene grains (one analysis per grain). Representative 2σ counting errors (in parentheses) are given for the first analysis. Wo, En and Fs are the proportions of Ca, Mg and Fe normalized to 100%; these are different than the projected values used in thermometric calculations (Andersen, Lindsley and Davidson, 1993)

Sample	KEH259A			KEH259E		KEH274B				KEH274D		KEH274F			KEH408	
Analysis #	2	3	5	2	5	3	4	5	6	2	3	2	4	6	4	5
SiO_2	51.34 (0.25)	51.52	51.54	50.74	51.99	51.02	51.68	51.94	51.91	51.36	51.28	51.29	50.46	50.98	52.25	51.74
Al_2O_3	3.22 (0.07)	3.24	3.02	3.06	2.97	2.95	3.11	3.04	3.01	3.09	3.04	2.91	2.92	2.87	2.46	2.95
FeO	6.71 (0.21)	7.17	7.27	6.82	7.73	7.39	6.98	6.90	7.08	7.74	7.71	7.46	8.53	8.02	7.22	7.38
MnO	0.09 (0.01)	0.20	0.01	0.26	0.23	0.12	0.12	0.16	0.15	0.10	0.15	0.17	0.17	0.19	0.15	0.00
MgO	15.86 (0.16)	15.83	15.79	15.26	16.66	16.01	15.89	16.08	15.93	15.98	16.09	15.19	16.03	16.12	16.20	16.12
CaO	21.14 (0.27)	20.50	20.36	21.99	20.51	19.60	20.82	20.59	20.86	20.17	20.02	20.72	18.66	19.34	20.46	20.15
Na_2O	0.31 (0.03)	0.32	0.33	0.35	0.36	0.38	0.37	0.34	0.35	0.36	0.38	0.37	0.36	0.35	0.34	0.37
TiO_2	0.93 (0.05)	0.92	0.96	0.96	0.94	1.19	1.25	1.14	1.21	1.16	1.17	1.14	1.27	1.17	0.93	1.28
Cr_2O_3	0.07 (0.01)	0.11	0.06	0.00	0.10	0.25	0.19	0.23	0.23	0.19	0.18	0.15	0.27	0.23	0.21	0.24
Total	99.67	99.81	99.34	99.44	101.49	98.91	100.41	100.42	100.73	100.15	100.02	99.40	98.67	99.27	100.22	100.23
Cations per 6 oxygens:																
Si	1.90	1.90	1.91	1.89	1.90	1.90	1.90	1.91	1.90	1.90	1.90	1.91	1.89	1.90	1.92	1.90
Al	0.14	0.14	0.13	0.13	0.13	0.13	0.14	0.13	0.13	0.14	0.13	0.13	0.13	0.13	0.11	0.13
Fe	0.21	0.22	0.23	0.21	0.24	0.23	0.22	0.21	0.22	0.24	0.24	0.23	0.27	0.25	0.22	0.23
Mn	0.00	0.01	0.00	0.01	0.01	0.00	0.00	0.01	0.01	0.00	0.01	0.01	0.01	0.01	0.01	0.00
Mg	0.88	0.87	0.87	0.85	0.91	0.89	0.87	0.88	0.87	0.88	0.89	0.84	0.90	0.89	0.89	0.88
Ca	0.84	0.81	0.81	0.88	0.80	0.78	0.82	0.81	0.82	0.80	0.80	0.82	0.75	0.77	0.81	0.79
Na	0.02	0.02	0.02	0.03	0.03	0.03	0.03	0.02	0.03	0.03	0.03	0.03	0.03	0.03	0.02	0.03
Ti	0.03	0.03	0.03	0.03	0.03	0.03	0.04	0.03	0.03	0.03	0.03	0.03	0.04	0.03	0.03	0.04
Cr	0.00	0.00	0.00	0.00	0.00	0.01	0.01	0.01	0.01	0.01	0.01	0.00	0.01	0.01	0.01	0.01
Wo	44.6	43.2	42.8	45.3	41.3	41.7	43.7	43.0	43.5	42.6	42.4	43.5	39.2	40.3	42.5	42.1
En	46.6	46.5	46.2	43.7	46.6	47.4	46.3	46.6	46.3	46.9	47.5	44.3	46.8	46.7	46.9	46.9
Fs	8.8	10.3	11.0	11.0	12.1	10.9	10.0	10.4	10.2	10.5	10.1	12.2	14.0	13.0	10.6	11.0

TABLE 4

Electron microprobe analyses of hornfelsic orthopyroxene grains (one analysis per grain). Representative 2σ counting errors (in parentheses) are given for the first analysis. Wo, En and Fs are the proportions of Ca, Mg and Fe normalized to 100%; these are different than the projected values used in thermometric calculations (Andersen, Lindsley and Davidson, 1993)

Sample	KEH259A		KEH259E		KEH274B		KEH274D		KEH274F				KEH408	
Analysis #	1	7	3	4	7	8	4	5	1	3	5	7	3	6
SiO_2	55.85 (0.27)	55.48	55.53	55.37	55.56	55.96	55.19	55.73	54.78	54.80	54.07	55.60	55.87	55.62
Al_2O_3	1.69 (0.06)	1.72	1.53	1.47	1.54	1.51	1.49	1.57	1.40	1.33	1.37	1.07	1.33	1.43
FeO	11.92 (0.28)	12.21	12.41	12.60	14.04	13.49	13.99	14.20	14.41	14.33	14.69	14.45	13.49	13.71
MnO	0.27 (0.04)	0.37	0.35	0.31	0.31	0.21	0.35	0.37	0.34	0.28	0.39	0.29	0.46	0.30
MgO	29.35 (0.22)	29.39	29.21	29.13	28.60	28.74	28.12	28.32	27.35	27.53	27.51	27.68	28.93	28.35
CaO	1.42 (0.07)	1.52	1.42	1.45	1.66	1.41	1.52	1.61	1.55	1.50	1.55	1.46	1.43	1.26
Na_2O	0.02 (0.00)	0.03	0.01	0.00	0.03	0.01	0.01	0.03	0.02	0.04	0.02	0.01	0.03	0.02
TiO_2	0.43 (0.03)	0.40	0.41	0.42	0.53	0.49	0.49	0.52	0.52	0.47	0.52	0.44	0.51	0.51
Cr_2O_3	0.00 (0.00)	0.01	0.03	0.07	0.05	0.13	0.10	0.08	0.00	0.05	0.04	0.09	0.06	0.11
Total	100.95	101.13	100.90	100.82	102.32	101.95	101.26	102.43	100.37	100.33	100.16	101.09	102.11	101.31
Cations per 6 Oxygens:														
Si	1.96	1.95	1.96	1.96	1.95	1.96	1.96	1.95	1.96	1.96	1.95	1.97	1.96	1.96
Al	0.07	0.07	0.06	0.06	0.06	0.06	0.06	0.07	0.06	0.06	0.06	0.04	0.06	0.06
Fe	0.35	0.36	0.37	0.37	0.41	0.40	0.41	0.42	0.43	0.43	0.44	0.43	0.40	0.41
Mn	0.01	0.01	0.01	0.01	0.01	0.01	0.01	0.01	0.01	0.01	0.01	0.01	0.01	0.01
Mg	1.54	1.54	1.53	1.53	1.49	1.50	1.48	1.48	1.46	1.47	1.48	1.46	1.51	1.49
Ca	0.05	0.06	0.05	0.06	0.06	0.05	0.06	0.06	0.06	0.06	0.06	0.06	0.05	0.05
Na	0.00	0.00	0.00	0.00	0.00	0.00	0.00	0.00	0.00	0.00	0.00	0.00	0.00	0.00
Ti	0.01	0.01	0.01	0.01	0.01	0.01	0.01	0.01	0.01	0.01	0.01	0.01	0.01	0.01
Cr	0.00	0.00	0.00	0.00	0.00	0.00	0.00	0.00	0.00	0.00	0.00	0.00	0.00	0.00
Wo	2.8	2.9	2.7	2.8	3.2	2.7	2.9	3.1	3.1	2.9	3.0	2.9	2.8	2.5
En	79.2	79.2	78.6	78.2	76.7	77.0	75.9	75.8	74.8	75.1	74.6	75.1	77.3	76.7
Fs	18.0	17.9	18.7	19.0	20.1	20.3	21.2	21.1	22.1	22.0	22.4	22.0	19.9	20.8

have been depleted in ^{18}O relative to typical unaltered basalts, but the plutonic rocks and xenoliths have markedly different plagioclase-pyroxene fractionation trends.

The gabbros and peridotites delineate a steeply dipping, disequilibrium fractionation trend characteristic of mafic plutonic rocks that have

TABLE 5

Metamorphic temperatures for metabasalt xenoliths from the Kap Edvard Holm Complex, calculated by two-pyroxene thermometry. Calculated assuming a pressure of 1.5 kb

Sample	Mineral*	Number of analyses	Non-quad. components (mol %)**	Temperature range (°C)	Average (°C)	Average, all analyses (°C)
KEH259A	cpx	3	11.0	1048-1064	1053	1056
	opx	2	4.9	1050-1071	1061	
KEH259E	cpx	2	13.6	1017-1131	1074	1062
	opx	2	4.3	1047-1052	1050	
KEH274B	cpx	4	11.2	1022-1077	1043	1048
	opx	2	4.9	1034-1084	1059	
KEH274D	cpx	2	12.3	1078-1091	1085	1073
	opx	2	4.7	1053-1068	1061	
KEH274F	cpx	3	11.7	994-1125	1075	1062
	opx	4	4.4	1037-1067	1052	
KEH408	cpx	2	10.1	1038-1057	1048	1035
	opx	2	4.5	1003-1040	1022	

* cpx = clinopyroxene, opx = orthopyroxene

** Average non-quadrilateral components (normative components other than wollastonite, enstatite, ferrosilite).

TABLE 6

*Strontium isotope analyses of metabasalt xenoliths and a layered olivine gabbro from Stand and Deliver Nunatak, Kap Edvard Holm Complex**

Sample	Description	$^{87}Sr/^{86}Sr$ **
KEH259A	Metabasalt xenolith, whole rock	0.703825 ± 8
KEH274D	Metabasalt xenolith, plagioclase separate	0.703404 ± 7
KEH303B	Metabasalt xenolith, plagioclase separate	0.704622 ± 7
KEH264B	Layered olivine gabbro, plagioclase separate	0.704513 ± 9

* Whole-rock Rb/Sr ratios were all <0.01 (Table 7 for xenoliths; Brandriss, 1993, for gabbro). Assuming ages of 50–60 Ma for the basalts and gabbros (Nielsen and others, 1981; Nevle and others, 1994), measured ratios are probably within 0.00005 of the initial values.

** Errors are in the last decimal place.

TABLE 7

Oxygen isotope analyses of minerals from cumulus and postcumulus plutonic rocks

Sample number and description		$\delta^{18}O$ plag	$\delta^{18}O$ px	$\delta^{18}O$ hb	$\delta^{18}O$ other	
LAYERED GABBROS						
KEH264B	Layered gabbro	4.6	4.5			
KEH270	Layered gabbro	3.3	3.8			
KEH400	Layered gabbro	-0.6	3.7			
KEH424	Layered gabbro	0.0	3.5			
KEH279	Layered gabbro	-3.7	4.0			
KEH283	Layered gabbro	-0.9	4.0			
KEH274A-1	Layered gabbro, <1.5 cm from xenolith KEH274A-2	-1.3	2.1			
KEH278	Layered gabbro, between two xenoliths 30 cm apart	0.7	2.9			
KEH303D	Layered gabbro,10 cm below xenolith KEH303	-4.1	2.8			
KEH303E	Layered gabbro	2.8	3.5			
KEH407	Mafic macrolayer	-2.6	2.8	3.0		
KEH412	Mafic macrolayer	3.2	3.1			
KEH425	Mafic macrolayer	-0.5	2.8			
PERIDOTITES (POSTCUMULUS)						
KEH303C	Large semi-conformable body, 0.5 m above xenolith KEH303	-1.4	2.2	2.3		
KEH303A	Large semi-conformable body, 1.5 m above KEH303C	-1.5	2.7			
KEH406A-2	Large semi-conformable body, <1.5 cm from xenolith KEH406A-1	-0.1	2.9			
KEH406B	Large semi-conformable body, 1.6 m above KEH406A	1.5	3.0	3.2		
KEH289	Small (20 cm) discordant pod	0.4	3.3			
COARSE-GRAINED GABBRO (POSTCUMULUS)						
KEH406C	Large semi-conformable body	-4.5	3.4			
KEH410A-2	Large semi-conformable body	-3.5	4.0			
KEH411	Large semi-conformable body	-4.2	3.5			
KEH414	Large semi-conformable body	-5.4	3.6	2.9	-5.5	(a+c)

plag = plagioclase; px = clinopyroxene; hb = magnesiohornblende (igneous); a+c = secondary actinolite + chlorite

All values are in per mil relative to SMOW. Values for plagioclase, pyroxene and hornblende are averages of two or more analyses, with reproducibilities typically better than +/− 0.2 per mil. Sample of actinolite + chlorite was analyzed only once.

exchanged oxygen with low-$\delta^{18}O$ hydrothermal fluids during subsolidus alteration (Forester and Taylor, 1977; Taylor and Forester, 1979; Gregory and Taylor, 1981; Ito and Clayton, 1983; Stakes and others, 1991; Kempton, Hawkesworth, and Fowler, 1991; Fehlhaber and Bird, 1991). This trend arises because water exchanges oxygen with plagioclase much

TABLE 8

Oxygen isotope analyses of minerals from metabasalt xenoliths and adjacent plutonic rocks, Stand and Deliver Nunatak

Sample number and description		$\delta^{18}O$ plag	$\delta^{18}O$ px	$\delta^{18}O$ hb
XENOLITHS:				
KEH259A	Pegmatitic pod			-6.0
KEH259D	Fine-grained leucosome	-3.9	-5.5	
KEH267B	Hornfels	-1.3	2.4	
KEH274A-2	Hornfels (0.01 m)*	-3.2	-3.5	
KEH274B	Hornfels (0.3 m)*	-3.9	-4.6	
KEH274F	Hornfels (0.8 m)*	-3.8	-4.3	
KEH274D	Hornfels (1.8 m)*	-4.2	-5.0	
KEH274F	Pegmatitic pod			-4.4
KEH302	Pegmatitic pod			-3.8
KEH303B	Hornfels	0.6	1.5	
KEH303G	Hornfels	0.4	0.7	
KEH403	Hornfels	-4.7	-5.1	
KEH406A-1	Hornfels	-1.7	-1.4	
KEH408	Hornfels	-5.2	-5.1	
PLUTONIC AND POSTCUMULUS ROCKS:				
KEH274A-1	Layered olivine gabbro 2 cm from KEH274A-2	-1.3	2.1	
KEH406A-2	Postcumulus peridotite 2 cm from KEH406A-1	-0.1	2.9	

* Distance from contact with gabbro.

plag = plagioclase; px = clinopyroxene, with minor orthopyroxene in some samples; hb = hornblende

All values are in per mil relative to SMOW. Each value is the average of two or more analyses, with reproducibilities typically better than +/− 0.2 per mil.

more rapidly than with pyroxene, producing disequilibrium ^{18}O fractionations between these minerals (Taylor, 1974; Criss, Gregory, and Taylor, 1987; Gregory, Criss, and Taylor, 1989).

Like the gabbros, the xenoliths have been depleted in ^{18}O relative to typical unaltered basalts, with $\delta^{18}O$ values for plagioclase and pyroxene as low as −5.2 and −5.5 permil, respectively. Unlike the gabbros, however, the xenoliths have plagioclase-pyroxene ^{18}O fractionations close to equilibrium values for the crystallization temperatures inferred from two-pyroxene thermometry (~1050°C; fig. 12). This implies that the xenoliths were nearly unaffected by oxygen isotope exchange during subsolidus hydrothermal alteration of the intrusion, an inference that is consistent with a notable scarcity of retrograde mineralogic alteration in the xenolith hornfelses (Brandriss, Bird, and O'Neil, 1992). The low $\delta^{18}O$ values

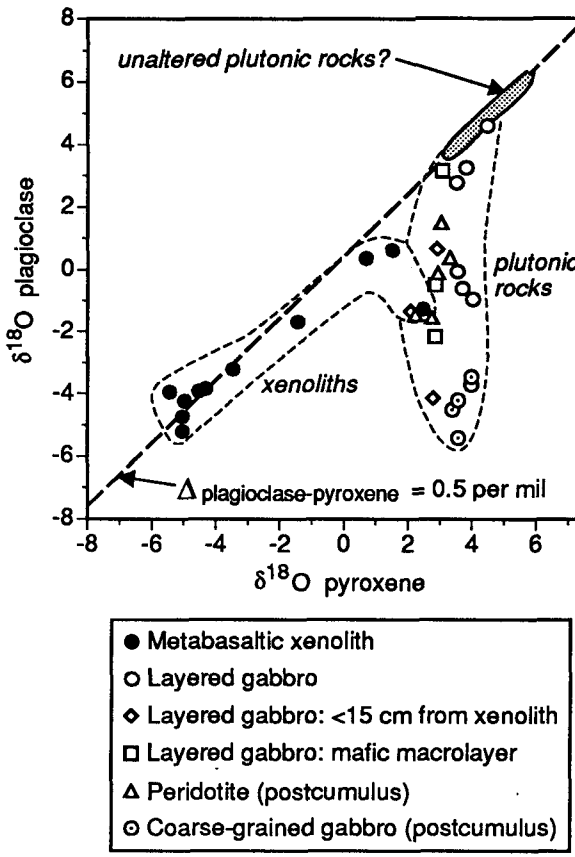

Fig. 12. Oxygen isotope compositions of plagioclase and pyroxene. The heavy dashed line represents equilibrium isotopic fractionation at approx 1050°C (Matthews, Goldsmith, and Clayton, 1983). The "unaltered gabbro" field includes typical values for fresh basalts from around the world (Taylor, 1974) but extends toward lower values to account for magmatic contamination of gabbros by low-^{18}O xenolithic material (as suggested by the slightly lower $\delta^{18}O_{pyroxene}$ values of gabbros collected near xenolith contacts).

of the hornfelses must therefore have been inherited from the country rock protoliths, indicating that the xenoliths underwent hydrothermal alteration and ^{18}O depletion *prior* to stoping and then recrystallized in isotopic equilibrium during high-temperature metamorphism within the intrusion. Like their altered and ^{18}O-depleted Lower Basalt protoliths, the low-$\delta^{18}O$ xenoliths probably contained hydrous secondary minerals at the time of stoping.

The resistance of the hornfelses to retrograde alteration and oxygen isotope exchange is probably attributable to rock texture. The hornfelses were altered much less pervasively than the gabbros, suggesting that the hornfelses were less susceptible to fluid infiltration at the scale of indi-

vidual mineral grains (Brandriss, Bird, and O'Neil, 1992). This could reflect a lesser tendency for the finer-grained and more regularly-textured hornfelses to develop permeable networks of grain-boundary microfractures. It must be noted that the near-equilibrium fractionations *cannot* be attributed to thorough subsolidus equilibration with low-$\delta^{18}O$ hydrothermal fluids at high-temperatures. Such a hypothesis would be inconsistent with the extensive isotopic disequilibrium *between* xenoliths (fig. 12) and would be difficult to reconcile with the extremely low susceptibility of the xenoliths to lower-temperature mineralogic alteration.

The postcumulus bodies of peridotite and the layered gabbros immediately adjacent to xenoliths tend to have $\delta^{18}O_{pyroxene}$ values slightly lower than those of the typical layered gabbros (fig. 12). This probably reflects minor contamination with low-^{18}O xenolithic material at magmatic temperatures.

Xenolith Hornfelses

Whole-rock compositions.—Whole-rock major and trace element compositions of xenolith hornfelses are presented in table 9. The hornfelses are compositionally diverse, but nearly all share a conspicuous feature: they are dramatically depleted in incompatible elements relative to the known compositional ranges of the Lower Basalt protoliths (figs. 13, 14). This suggests that the xenoliths were partially melted, leaving refractory solid residua after melt extraction. Large-ion-lithophile elements (Ba, Rb, K, Th, Y, REE) and high-field-strength elements (Nb, P, Zr, Hf) are depleted by factors of three to ten relative to the great majority of Lower Basalt lavas. Strontium and titanium, though often described as "incompatible" elements, have not been strongly depleted due to their tendency to partition into abundant minerals in the hornfelsed residua (Sr into plagioclase, Ti into magnetite, ilmenite and clinopyroxene; Henderson, 1982; Nielsen, 1992).

The general pattern of incompatible element depletion is characteristic of all but one of the analyzed hornfels samples. The exception, sample KEH274D, is from the center of a tabular xenolith 4 m thick. Concentrations of incompatible elements in this sample are within or only slightly below the ranges for the Lower Basalts, suggesting that the rock underwent little if any melting. Toward the rim of the xenolith, the hornfels becomes more depleted in incompatible elements and more enriched in highly compatible elements (fig. 15), reflecting a greater degree of melting (or melt extraction) toward the xenolith margin.

The concentrations of major elements and compatible trace elements in the xenoliths overlap the ranges for the Lower Basalts (fig. 13). On average, the xenoliths are poorer in Si, Al, Na, K, and P and slightly richer in Mg, Fe, Cr, and Ni than are the Lower Basalt country rocks. This is potentially consistent with extraction of felsic or dioritic melts from the basaltic protoliths. Alternatively, most of the differences (except

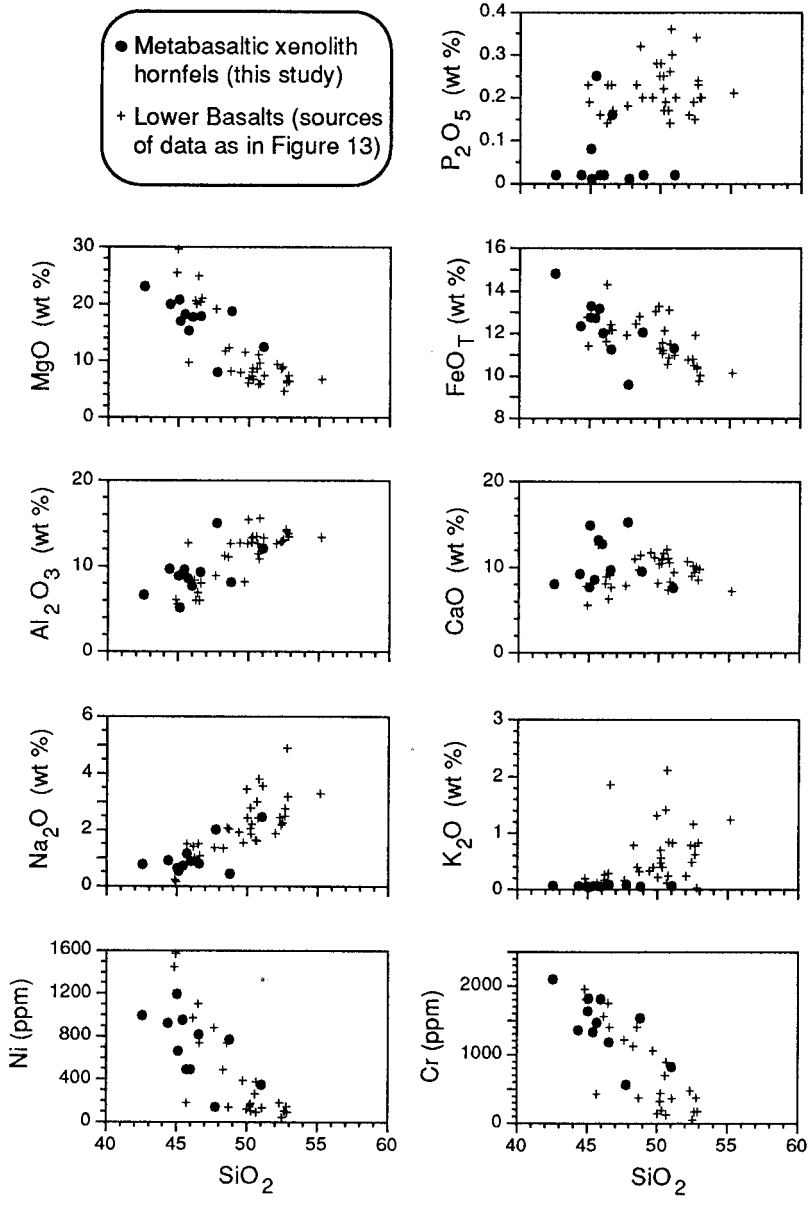

Fig. 13. Concentrations of major elements and compatible trace elements in metabasaltic xenoliths and Lower Basalt country rocks. Data for the Lower Basalts are compiled from Gill and others (1988 and unpublished data) and Holm (1988 and unpublished data).

TABLE 9

Compositions of metabasaltic xenoliths from Stand and Deliver Nunatak

	Granoblastic hornfels						
Sample	KEH259A	KEH267B	KEH274A 0-1 cm*	KEH274B 30 cm*	KEH274C 90 cm*	KEH274D 180 cm*	KEH303G
SiO_2	48.78	45.99	42.57	45.04	46.56	45.44	45.69
TiO_2	1.01	0.73	0.71	1.56	1.97	2.13	1.20
Al_2O_3	8.09	7.65	6.66	8.90	9.29	9.62	8.59
Fe_2O_3	13.52	13.50	16.62	14.32	12.63	14.31	14.78
MnO	0.23	0.21	0.24	0.18	0.17	0.19	0.22
MgO	18.70	17.75	23.03	20.68	17.85	18.18	15.32
CaO	9.55	12.69	8.08	7.69	9.70	8.58	13.15
Na_2O	0.41	0.87	0.75	0.63	0.78	0.72	1.14
K_2O	0.05	0.05	0.06	0.05	0.09	0.06	0.06
P_2O_5	0.02	0.02	0.02	0.08	0.16	0.25	0.02
Total	100.36	99.46	98.74	99.13	99.20	99.48	100.17
Zn	112	78	127	105	91	111	79
Cu	28	25	25	77	130	207	12
Ni	764	485	989	1195	811	950	486
Cr	1531	1805	2092	1627	1175	1327	1465
V	174	243	203	253	272	319	331
Co	90	95				95	83
Sc	26	42				26	44
Ba	b.d.	30	b.d.	35	55	42	27
Rb	1	b.d.	b.d.	b.d.	2	1	b.d.
Th	b.d.	b.d.	b.d.	b.d.	b.d.	2	b.d.
U	1	b.d.	b.d.	b.d.	b.d.	1	b.d.
Nb	1	1	1	3	5	6	1
Ta	1	1				1	b.d.
Sr	134	154	158	158	220	216	182
Zr	13	10	16	62	86	127	14
Hf	b.d.	b.d.				3	1
Pb	4	5	1	b.d.	3	6	4
Ga	14	11	17	17	17	18	12
La	1.05	0.87				6.30	1.30
Ce	3.70	3.60				19.20	3.60
Sm	0.90	1.22				4.04	1.45
Eu	0.43	0.40				1.43	0.49
Tb	0.23	0.25				0.75	0.20
Yb	0.57	0.38				1.69	0.44
Lu	0.098	0.058				0.27	0.066
Y	7	8	13	13	19	23	10

TABLE 9
(continued)

	Granoblastic hornfels				Leucosome	Gabbroic stringer
Sample	KEH401	KEH403	KEH406A	KEH408	KEH259D	KEH303B
SiO_2	51.04	45.12	47.78	44.37	42.52	42.43
TiO_2	1.69	1.44	1.65	1.44	1.48	1.84
Al_2O_3	12.07	5.16	14.99	9.66	20.40	6.62
Fe_2O_3	12.69	14.93	10.78	13.88	16.74	18.82
MnO	0.19	0.25	0.14	0.19	0.09	0.25
MgO	12.40	16.94	7.93	19.90	4.08	17.24
CaO	7.59	14.83	15.20	9.25	12.64	11.81
Na_2O	2.45	0.51	2.00	0.88	2.19	0.74
K_2O	0.06	0.04	0.09	0.06	0.12	0.06
P_2O_5	0.02	0.01	0.01	0.02	0.02	0.02
Total	100.20	99.23	100.57	99.65	100.28	99.83
Zn	116	106	58	96	80	121
Cu	22	40	12	26	63	40
Ni	344	662	140	921	117	543
Cr	820	1812	562	1354	48	2023
V	229	301	470	200	279	576
Co					65	113
Sc					17	39
Ba	42	12	55	b.d.	46	18
Rb	b.d.	b.d.	b.d.	b.d.	1	1
Th	b.d.	2	b.d.	b.d.	b.d.	1
U	b.d.	b.d.	b.d.	b.d.	2	1
Nb	2	1	1	1	1	2
Ta					b.d.	b.d.
Sr	254	82	318	184	587	135
Zr	28	24	23	30	b.d.	20
Hf					b.d.	b.d.
Pb	2	2	2	b.d.	7	4
Ga	19	10	19	17	26	12
La					1.20	1.80
Ce					2.70	6.40
Sm					0.43	1.78
Eu					0.34	0.70
Tb					0.078	0.29
Yb					0.21	0.95
Lu					0.045	0.16
Y	7	10	11	9	3	12

Oxides in weight percent, elements in ppm. b.d. = below detection. Th, Hf, Ta, Co, Sc, and REE by INAA; all other elements by XRF.
* Distance from contact with gabbro.

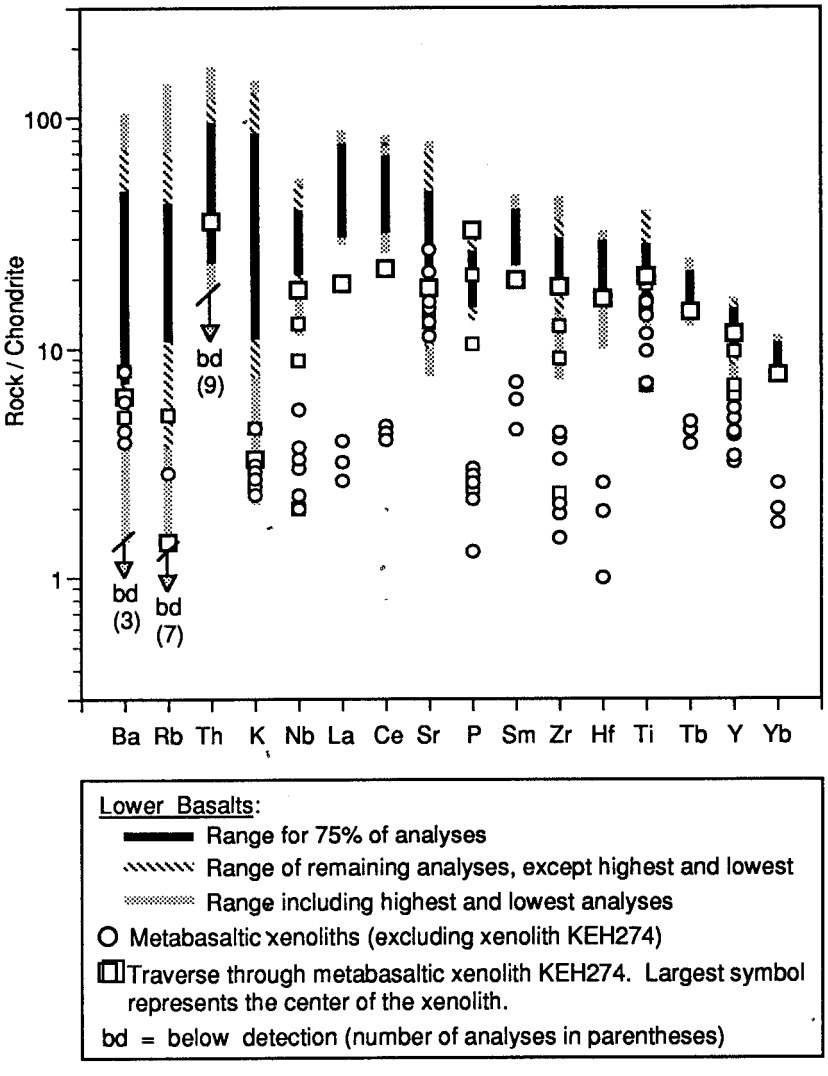

Fig. 14. Concentrations of incompatible elements in metabasaltic xenolith hornfelses, and Lower Basalt country rocks. Data for the Lower Basalts are compiled from Gill and others (1988 and unpublished data) and Holm (1988 and unpublished data), with an additional sample (1133, table 1) from Brandriss (ms) and Manning and Bird (1995).

for the strong incompatible element depletions) could reflect derivation of the xenoliths from relatively primitive units of the Lower Basalts.

Mineral compositions.—Representative electron microprobe analyses of pyroxene, olivine and plagioclase are presented in tables 3, 4, 10 and 11. Complete tabulations are given in Brandriss (ms) together with

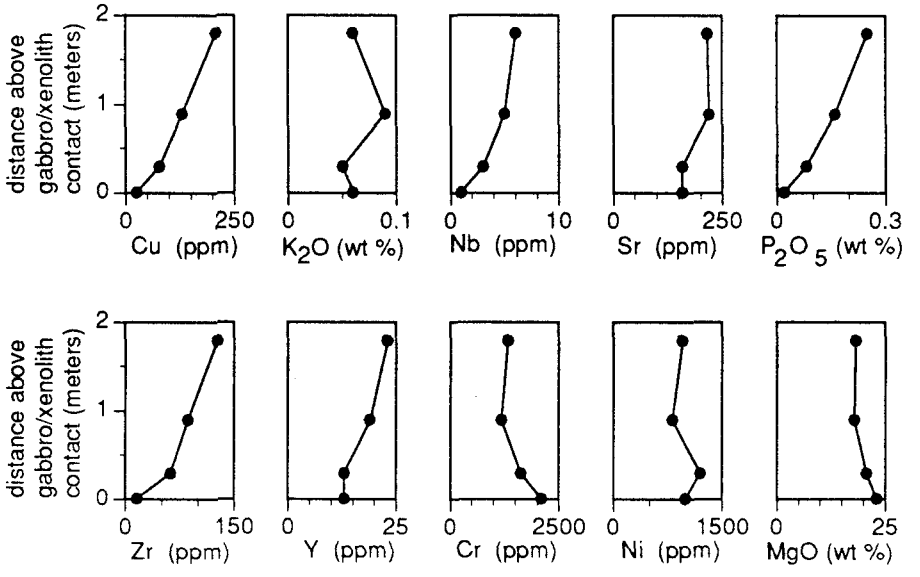

Fig. 15. Whole-rock compositions of metabasaltic hornfels in a core-to-rim traverse through a 4-m-thick xenolith (samples KEH274A-D).

analyses of minerals in the layered gabbros. Analyses of pegmatitic phlogopite and hornblende (magnesio-hastingsite) are given in Brandriss and others (1995).

In most cases, minerals in the xenoliths are compositionally distinct from those in the gabbros. Olivine and augite are more magnesian in the xenoliths: forsterite contents of olivine range from Fo_{72} to Fo_{78} in xenoliths and from Fo_{70} to Fo_{74} in gabbros, and Mg/(Mg + Fe) ratios in augite range from 0.78 to 0.80 in xenoliths and from 0.76 to 0.78 in gabbros. Plagioclase in the xenoliths is typically more calcic than in the gabbros (up to An_{74} in xenoliths versus $An_{63\text{-}68}$ in gabbros), but in a few cases it is more sodic (as low as An_{58}). The compositional differences between minerals in the xenoliths and adjacent gabbros reflect chemical disequilibrium at the scale of meters. Analyses of minerals from different parts of a single xenolith indicate that disequilibria can persist to within a few millimeters of gabbro/xenolith contacts (fig. 16).

Pegmatitic, Leucocratic and Gabbroic Bodies

Many xenoliths enclose bodies of material that crystallized wholly or partially from silicate liquids derived by partial melting. These bodies include:

1. Pegmatitic pods rich in hornblende and phlogopite (fig. 2).
2. Plagioclase-rich leucosomes, locally containing pockets of hornblende-rich pegmatite (figs. 7, 8).
3. Bands, wisps, and pods of olivine gabbro (fig. 6).

TABLE 10

Representative analyses of hornfelsic olivine from metabasalt xenoliths, with analyses from layered gabbros for comparison. Fo and Fa are molar proportions of Mg and Fe, normalized to 100%

	Xenolith hornfelses						*Layered gabbros*	
Sample	*KEH 267A*	*KEH 274A*	*KEH 274B*	*KEH 274C*	*KEH 303B*	*KEH 408*	*KEH 264B*	*KEH 424*
SiO_2	38.26	38.82	38.87	38.83	38.81	38.63	38.36	37.80
MgO	36.95	38.21	40.48	39.84	36.20	39.64	36.35	36.11
FeO	24.94	22.00	20.78	21.02	25.19	21.34	26.24	27.31
MnO	0.35	0.21	0.25	0.26	0.45	0.27	0.43	0.47
NiO	0.00	0.00	0.10	0.51	0.34	0.21	0.04	0.05
Total	100.50	99.24	100.48	100.46	100.99	100.09	101.42	101.74
Cations per 4 oxygens:								
Si	1.00	1.01	1.00	1.00	1.01	1.00	1.00	0.99
Mg	1.44	1.49	1.55	1.53	1.41	1.53	1.41	1.41
Fe	0.55	0.48	0.45	0.45	0.55	0.46	0.57	0.60
Mn	0.01	0.00	0.01	0.01	0.01	0.01	0.01	0.01
Ni	0.00	0.00	0.00	0.01	0.01	0.00	0.00	0.00
Fo	72.5	75.6	77.6	77.2	71.9	76.8	71.2	70.2
Fa	27.5	24.4	22.4	22.8	28.1	23.2	28.8	29.8

Pegmatitic pods.—Many of the large xenoliths contain discrete pods of pegmatite scattered in the mafic hornfels. These pods are centimeters to tens of centimeters in size and usually occur in swarms, most commonly near the centers of xenoliths (fig. 2). They consist mainly of hornblende, plagioclase, phlogopite, and apatite with minor amounts of ilmenite and clinopyroxene. A euhedral crystal of zircon was found in one sample.

The pods have igneous textures. Euhedral apatite grains are enclosed in euhedral megacrysts of hornblende and phlogopite, and plagioclase is present as fine- to medium-grained intergranular aggregates of subhedral to euhedral prisms (some of which are compositionally zoned). Hornblende at the margins of the pods has grown outward and enveloped hornfelsic mineral grains (fig. 17). Some hornblende megacrysts contain scattered irregular blebs of augite that are optically continuous over several centimeters. These appear to be the vestiges of early-formed pyroxene crystals that were replaced by igneous hornblende during cooling.

Measured $\delta^{18}O$ values of the hornblende megacrysts range from −6.0 to −3.8 permil. A few centimeters from one megacryst (KEH274F, $\delta^{18}O = -4.4$ permil) the hornfelsic pyroxene and plagioclase have $\delta^{18}O$ values of −4.3 and −3.8 permil respectively. The isotopic fractionations between these three minerals are close to equilibrium values for magmatic temperatures (Bottinga and Javoy, 1975), implying that the horn

TABLE 11

Representative analyses of hornfelsic plagioclase from metabasalt xenoliths, with analyses from layered gabbros for comparison. Also shown are analyses from a xenolith rim and the adjacent gabbro (KEH274A). An, Ab and Or are molar proportions of Ca, Na and K normalized to 100%

	Xenolith hornfelses				*Layered gabbros*		*Gabbro*	*Xenolith*
Sample	*KEH 259E*	*KEH 274F*	*KEH 274G*	*KEH 303B*	*KEH 264B*	*KEH 424*	*KEH 274A*	
SiO_2	49.82	48.76	49.98	50.28	51.46	52.04	52.48	52.68
Al_2O_3	32.68	32.19	31.49	31.05	29.88	30.34	29.49	29.47
FeO	0.79	0.59	0.56	0.62	0.30	0.57	0.52	0.43
MgO	0.06	0.04	0.00	0.05			0.04	0.06
CaO	14.90	14.79	14.16	13.77	12.80	13.08	12.70	12.70
Na_2O	2.90	2.94	3.04	3.27	4.05	3.86	4.31	4.16
K_2O	0.06	0.15	0.15	0.08	0.23	0.25	0.24	0.23
Total	101.21	99.46	99.38	99.12	98.72	100.14	99.78	99.73
Cations per 8 oxygens:								
Si	2.25	2.24	2.29	2.31	2.37	2.36	2.39	2.40
Al	1.74	1.75	1.70	1.68	1.62	1.62	1.58	1.58
Fe	0.03	0.02	0.02	0.02	0.01	0.02	0.02	0.02
Mg	0.00	0.00	0.00	0.00			0.00	0.00
Ca	0.72	0.73	0.70	0.68	0.63	0.64	0.62	0.62
Na	0.25	0.26	0.27	0.29	0.36	0.34	0.38	0.37
K	0.00	0.01	0.01	0.00	0.01	0.01	0.01	0.01
An	73.7	72.9	71.4	69.6	62.8	64.2	61.1	62.0
Ab	25.9	26.2	27.7	29.9	35.9	34.3	37.5	36.7
Or	0.4	0.0	0.9	0.5	1.3	1.5	1.4	1.3

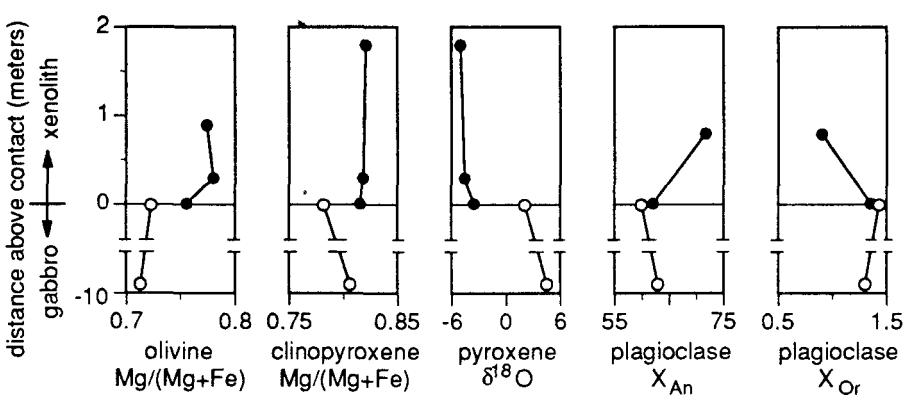

Fig. 16. Mineral compositions in a traverse across the contact between a xenolith (KEH274A-F) and the underlying gabbro. Compositions of gabbro minerals (open symbols) are from Brandriss (ms); gabbro samples are KEH274A-1 (at the contact) and KEH264B (at 9 m).

Fig. 17. Contact between a pegmatitic pod (left) and xenolith hornfels (right). A hornblende megacryst (dark gray) has engulfed rounded hornfels grains during growth. A euhedral crystal of apatite (a) is surrounded by saussuritized plagioclase. Field of view is 14 mm wide.

Fig. 18. Hornfelsed xenolith (sample KEH259A) with foliations deflected around hornblende boudins. Hornblende is present as dark cm-scale crystals (at center) and as bands of smaller crystals in the plane of foliation.

blende and hornfels crystallized at high temperature from the same reservoir of low-$\delta^{18}O$ xenolithic material. This is consistent with formation of the pegmatites from partial melts of the metabasalts. The preservation of high-temperature fractionations during cooling is attributable to the resistance of the hornfels and hornblende to subsolidus oxygen isotope exchange (Brandriss and others, 1992).

The pegmatitic plagioclase is relatively poor in calcium. Compositions in one pegmatite (KEH274F) range from An_{34} to An_{50} while compositions in the adjacent hornfels range from An_{70} to An_{73} (table 12). This suggests that the pegmatites crystallized from anatectic melts that had separated from the hornfelsed residuum. This is consistent with the high abundances of phlogopite and apatite, both of which are rich in incompatible elements. The hornfelses near some pegmatites contain plagioclase grains that are compositionally zoned, suggesting that melt extraction was incomplete.

TABLE 12

Representative analyses of plagioclase grains in a pegmatitic pod and the adjacent mafic hornfels. An, Ab and Or are the molar proportions of Ca, Na and K normalized to 100%

Sample	*KEH274F*						
Rock Type	*Pegmatite*			*Mafic hornfels*			
*Description**	*peg*	*peg*	*peg*	*fg*	*fg*	*relict*	*relict*
Analysis #	*25*	*26*	*27*	*32*	*33*	*30*	*31*
SiO_2	53.54	58.91	56.31	50.51	48.76	50.36	49.91
Al_2O_3	28.35	25.38	26.98	31.56	32.19	31.99	31.94
FeO	0.54	0.47	0.54	0.57	0.59	0.49	0.63
MgO	0.01	0.07	0.07	0.04	0.04	0.04	0.05
CaO	10.34	7.04	8.92	14.31	14.79	14.49	14.75
Na_2O	5.33	7.36	6.27	3.22	2.94	3.18	2.90
K_2O	0.46	0.39	0.23	0.16	0.15	0.00	0.12
Total	98.57	99.62	99.32	100.37	99.46	100.55	100.30
Cations per 8 Oxygens:							
Si	2.46	2.65	2.55	2.30	2.24	2.28	2.27
Al	1.53	1.34	1.44	1.69	1.75	1.71	1.71
Fe	0.02	0.02	0.02	0.02	0.02	0.02	0.02
Mg	0.00	0.00	0.00	0.00	0.00	0.00	0.00
Ca	0.51	0.34	0.43	0.70	0.73	0.70	0.72
Na	0.47	0.64	0.55	0.28	0.26	0.28	0.26
K	0.03	0.02	0.01	0.01	0.01	0.00	0.01
An	50.3	33.8	43.4	70.4	72.9	71.6	73.2
Ab	47.0	64.0	55.3	28.7	26.2	28.4	26.1
Or	2.7	2.2	1.3	0.9	0.0	0.0	0.7

* peg = anhedral pegmatitic; fg = fine-grained granoblastic; relict = relict hornfels crystals enclosed in pegmatitic hornblende (e.g. Figure 18).

One xenolith (KEH259A) contains pegmatitic hornblende crystals that form augen in a foliated hornfelsic matrix (fig. 18). Late intergranular plagioclase, abundant in the other pegmatites, is sparse or absent. Some of the hornblende crystals enclose euhedral apatite and plagioclase, and some are overgrown by phlogopite, producing textures suggestive of crystallization from a silicate liquid. The scarcity of late intergranular plagioclase, however, together with the deformation of the hornfels around hornblende megacrysts, suggest that much of this liquid was extracted during compaction of the partially fused xenolith. The ability of the plagioclase-rich liquids to segregate during deformation is demonstrated by the accumulation of plagioclase in pressure shadows adjacent to hornblende megacrysts (fig. 2).

Leucosomes.—Plagioclase-rich leucosomes are present in a variety of irregular forms, ranging from pods and lenses only centimeters in length to sheets as large as tens of centimeters thick and tens of meters long. Many of the smaller leucosomes are located along contacts between lava flows within xenoliths (fig. 8).

The xenolith that contains hornblende augen also contains a prominent leucosome. This leucosome, which was studied in detail, forms a sheet 30 m long (fig. 7; samples KEH259, KEH263). It is roughly coplanar with foliations in the host hornfels and is truncated sharply at the xenolith margin. The leucosome locally brecciates the hornfels (fig. 7) and is therefore inferred to have been a molten body. It is texturally and mineralogically heterogeneous and consists of decimeter-sized hornblende-rich pegmatitic patches in a fine-grained hornblende-free matrix (fig. 19A). Plagioclase and pyroxene from the matrix have low $\delta^{18}O$ values (-3.9 and -5.5 permil respectively) indicative of derivation from ^{18}O-depleted metabasalt.

The pegmatitic zones of the leucosome have igneous textures similar to those of the pegmatitic pods already described. Plagioclase crystals commonly have euhedral compositional zoning. Some hornblende megacrysts contain scattered but optically continuous blebs of clinopyroxene, suggesting that early-formed pyroxene was replaced by igneous hornblende during cooling. Such retrograde magmatic replacements, as well as the euhedral compositional zoning in plagioclase, are considered by Ashworth and McLellan (1985) to be reliable evidence for crystallization from silicate liquids.

The fine-grained parts of the leucosome have porphyritic or porphyroblastic textures in which ~5 mm crystals of subhedral to anhedral plagioclase and augite are set in a decussate matrix of ~0.2 mm grains (fig. 19B). Many large plagioclase crystals are compositionally zoned, with rims up to 10 percent more albitic than cores (fig. 19B, table 13). The rims are almost identical in composition to the plagioclase in the fine-grained matrix, whereas the cores are commonly of the same composition as plagioclase in the host mafic hornfels (table 13). These relationships are consistent with the leucosomes having crystallized from liquids that segregated from the hornfels. It is possible that the porphyritic

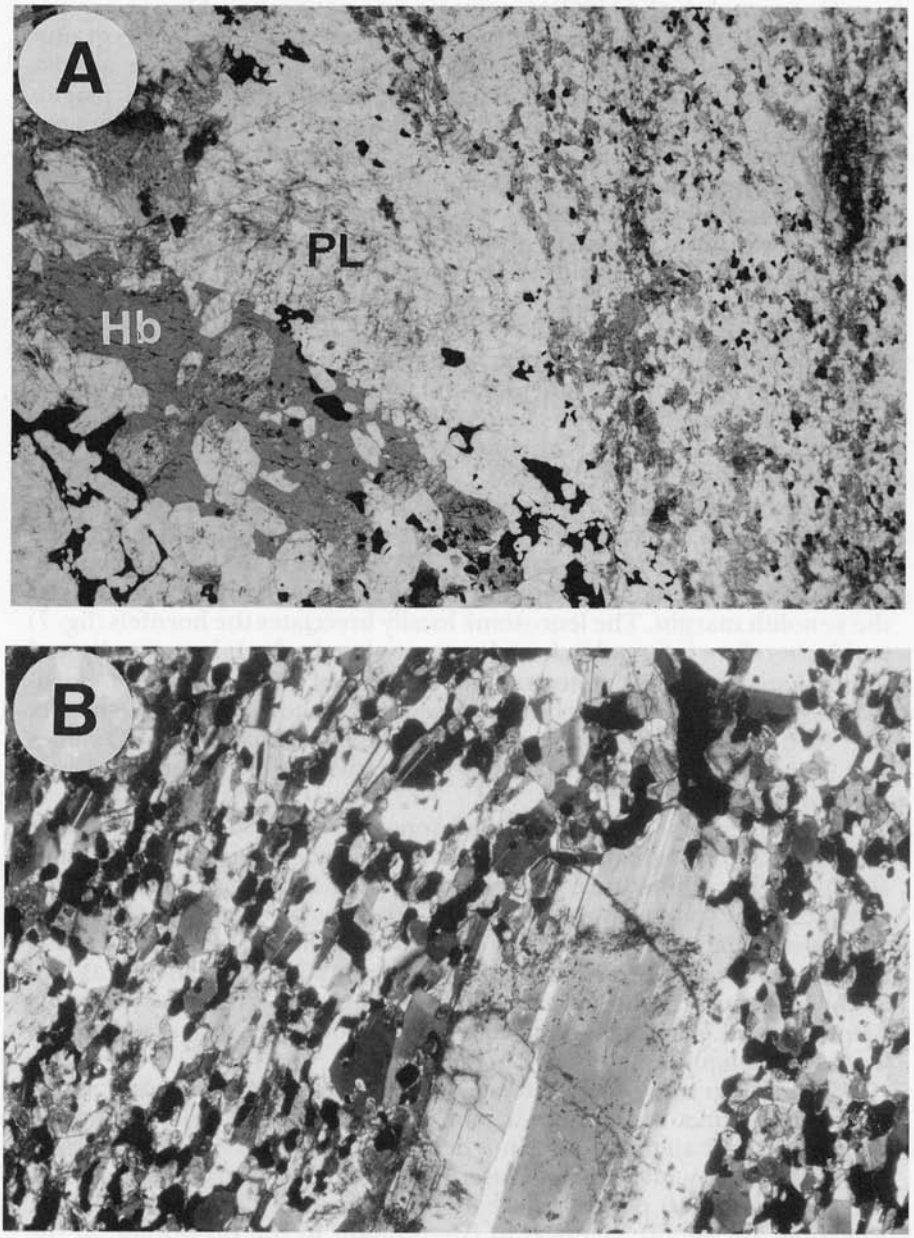

Fig. 19. Two samples of the leucosome shown in figure 7, collected 5 m apart. (A) Fine-grained and pegmatitic zones (sample KEH263). Hb = poikilitic hornblende, PL = plagioclase. Field of view is 14 mm wide. (B) Fine-grained zone with compositionally zoned plagioclase (sample KEH259D). Field of view is 6 mm wide.

TABLE 13

Representative analyses of plagioclase grains in two samples from a xenolith leucosome and the adjacent mafic hornfels. An, Ab and Or are molar proportions of Ca, Na and K normalized to 100%

Sample	*KEH259E*								*KEH263*					
Rock type	*Mafic hornfels*	*Leucosome (fine-grained zone)*							*Leucosome (pegmatitic zone)*			*Leucosome (fine-grained zone)*		
*Description**	*fg*	*fg*	*fg*	*porph*	*porph*	*porph*	*porph (core)*	*porph (rim)*	*peg*	*peg*	*peg*	*fg*	*fg*	*porph*
Analysis #	*108*	*114*	*115*	*113*	*116*	*110*	*112*	*111*	*1*	*2*	*6*	*4*	*5*	*3*
SiO_2	49.82	51.91	51.32	49.38	48.41	51.43	49.68	52.01	47.73	48.03	47.96	47.73	47.44	48.58
Al_2O_3	32.68	31.02	30.78	32.33	32.77	30.66	32.37	31.27	33.03	31.99	33.02	32.74	32.49	32.69
FeO	0.79	0.73	0.69	0.79	0.72	0.69	0.66	0.64	0.69	0.71	0.67	0.77	0.76	0.75
MgO	0.06	0.05	0.07	0.00	0.06	0.07	0.05	0.07	0.05	0.04	0.03	0.07	0.06	0.04
CaO	14.90	13.14	12.87	14.68	15.33	13.06	14.66	13.09	16.55	15.99	16.00	16.03	16.13	15.99
Na_2O	2.90	3.98	4.06	2.96	2.62	3.76	2.83	3.84	1.99	2.19	2.14	2.06	2.12	2.31
K_2O	0.06	0.09	0.08	0.06	0.05	0.10	0.06	0.06	0.08	0.14	0.10	0.09	0.04	0.10
Total	101.21	100.92	99.87	100.20	99.96	99.77	100.31	100.98	100.12	99.09	99.92	99.49	99.04	100.46
Cations per 8 Oxygens:														
Si	2.25	2.34	2.34	2.25	2.22	2.34	2.26	2.34	2.19	2.23	2.20	2.20	2.20	2.22
Al	1.74	1.65	1.65	1.74	1.77	1.65	1.74	1.66	1.79	1.75	1.79	1.78	1.78	1.76
Fe	0.03	0.03	0.03	0.03	0.03	0.03	0.02	0.02	0.03	0.03	0.03	0.03	0.03	0.03
Mg	0.00	0.00	0.00	0.00	0.00	0.00	0.00	0.00	0.00	0.00	0.00	0.00	0.00	0.00
Ca	0.72	0.63	0.63	0.72	0.75	0.64	0.72	0.63	0.81	0.79	0.79	0.79	0.80	0.78
Na	0.25	0.36	0.36	0.26	0.23	0.33	0.25	0.34	0.18	0.20	0.19	0.18	0.19	0.20
K	0.00	0.00	0.00	0.00	0.00	0.01	0.00	0.00	0.00	0.01	0.01	0.01	0.01	0.01
An	73.7	64.3	63.4	73.0	76.2	65.4	73.8	65.1	81.7	79.5	80.0	80.7	80.6	78.8
Ab	25.9	35.2	36.1	26.6	23.5	34.0	25.8	34.5	17.8	19.7	19.4	18.8	19.2	20.6
Or	0.4	0.5	0.5	0.4	0.3	0.6	0.4	0.4	0.5	0.8	0.6	0.5	0.2	0.6

* fg = fine-grained granoblastic; porph = large porphyritic or porphyroblastic crystal; peg = euhedral crystal in pegmatitic hornblende.

textures of the fine-grained zones were produced by quenching of the liquids, perhaps due to loss of volatiles via some indeterminate process. Such an explanation is suggested by the presence of primary hydrous minerals in the pegmatitic zones and their absence in the fine-grained zones.

Despite evidence for an anatectic origin, the leucosome is compositionally unlike any anatectic liquid produced experimentally by partial melting of basalt (Holloway and Burnham, 1972; Helz, 1976; Dixon and Rutherford, 1979; Spulber and Rutherford, 1983; Beard and Lofgren, 1991; Sisson and Grove, 1993). It is extremely rich in iron and aluminum, has a very high Fe/Mg ratio, and is extremely poor in silica and incompatible trace elements (table 9). This suggests that the leucosome cannot simply represent a bulk liquid produced by metabasalt melting. Instead, it probably crystallized from a late-stage liquid that formed only after substantial amounts of siliceous melt had already been expelled. The rare earth element pattern of the leucosome has a negative slope and positive Eu anomaly (fig. 20). These REE characteristics are typical of plagioclase-rich solid fractionates, suggesting that the leucosome itself is

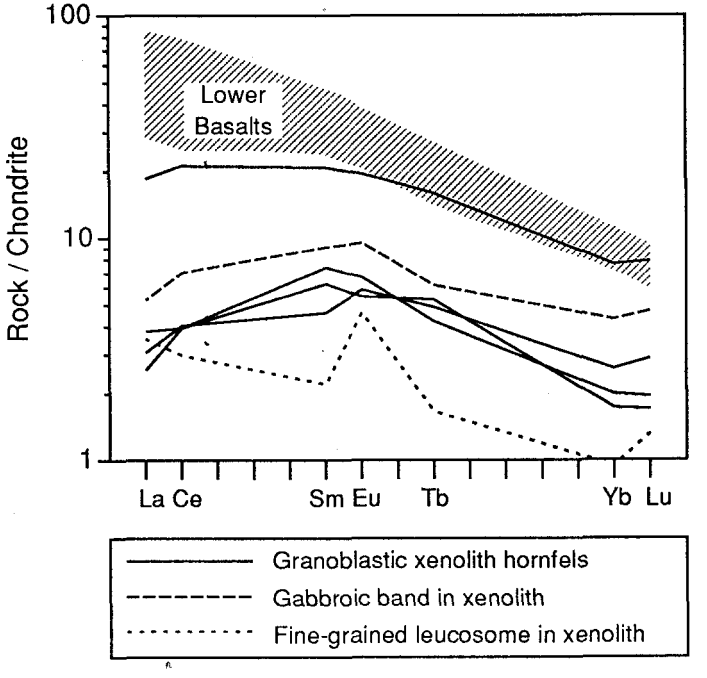

Fig. 20. Chondrite-normalized whole-rock REE patterns for xenoliths and Lower Basalt country rocks. Chondrite normalization factors are from Wakita and others (1971); the field for the Lower Basalts is mainly from Gill and others (1988) but has been expanded slightly downward by inclusion of sample 1133 (table 1).

to some extent a cumulate or residuum from which liquid has been removed.

Gabbroic bodies.—Many of the xenoliths contain bands, pods, or wisps of medium-grained ophitic gabbro consisting of plagioclase (commonly zoned), clinopyroxene, olivine, and magnetite (fig. 6). These bodies do not appear to be fingers or apophyses of the host gabbro but instead appear to have formed by *in situ* partial melting of the host xenoliths. Their distribution may reflect heterogeneities in the metabasaltic protoliths, with melting perhaps having been locally facilitated by concentrations of hydrous secondary minerals. The whole-rock composition of a typical gabbroic band (sample KEH303B) was measured and found to be depleted in incompatible elements relative to typical Lower Basalts (table 9; fig. 20). This suggests that some amount of melt rich in incompatible components was expelled during melting or recrystallization.

DISCUSSION

From chemical data and field relationships we have inferred that: (1) metabasaltic xenoliths in the study area were altered by meteoric-hydrothermal fluids prior to stoping; (2) most of the xenoliths were dehydrated and partially melted, leaving refractory hornfelsed residua; (3) some partial melts were trapped within xenoliths, where they crystallized; (4) other hydrous melts or fluids were expelled from the xenoliths, and in some places reacted with the host gabbroic cumulates. In the following sections, field and geochemical data will be combined with simple physical and chemical models to elucidate the timing and mechanisms of these processes.

Thermal Constraints on Dehydration and Melting

Thermal-mechanical models predict that sudden emplacement of a pluton into cool shallow crust will rapidly generate thermal stresses large enough to shatter the surrounding wall rocks, resulting in the stoping of relatively cold xenoliths into the magma (Marsh, 1982; Furlong and Myers, 1985). Heating of such xenoliths can, to a first approximation, be modeled as a conductive heat transfer problem (Marsh, 1982; Furlong and Myers, 1985). If a xenolith is assumed to be a sphere or an infinite slab and heats of fusion are ignored, then temperature profiles through the xenolith at various times can be calculated from analytical solutions to the heat flow equation using equations 3.4.4 and 9.3.4 of Carslaw and Jaeger (1959) or the corresponding graphical solutions presented in their figures 11 and 29. We have performed sample calculations for a spherical xenolith 4 m in diameter and a tabular xenolith 4 m thick (modeled as an "infinite slab") assuming an initial temperature of 400°C for the xenoliths, a constant temperature of 1050°C for the magma, and a thermal diffusivity of 0.005 cm^2/sec for rock and magma (Petrunin, Yurchak, and Tkach, 1971). Results are shown in figure 21.

The center of the xenolith reaches 1000°C within a few weeks in the case of the sphere and a few months in the case of the slab. Such rapid

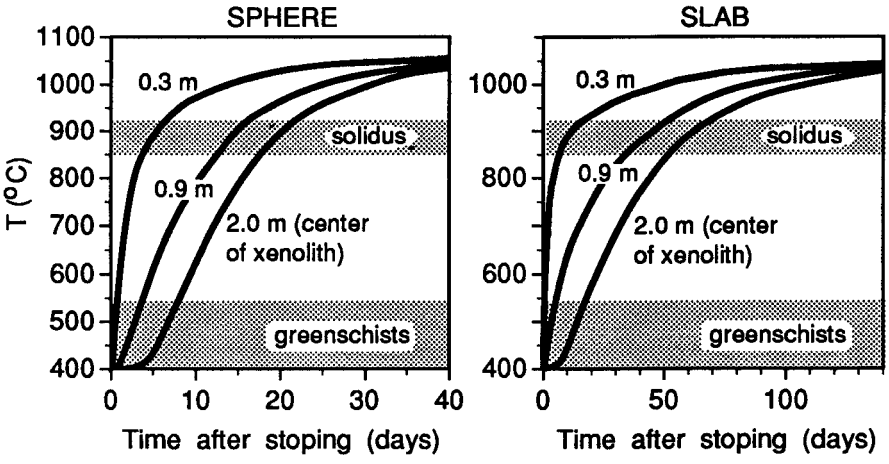

Fig. 21. Models for conductive heating of a spherical xenolith 4 m in diameter (left) and a tabular xenolith 4 m thick (right; modeled as an infinite slab). Labels on the curves are distances from the contact with gabbro. Note different scales on the x axes. The greenschist stability field is from Liou, Kuniyoshi, and Ito (1974); the solidus field is for hydrous basalt at ~2 kb (e.g. Beard and Lofgren, 1991).

heating would almost certainly have caused pervasive hydrofracturing of greenschist metabasalts due to overpressures generated by the coalescence and thermal expansion of fluids released during breakdown of chlorite, actinolite and epidote (Knapp and Knight, 1977). This hydrofracturing would probably have produced a permeable network of pores through which the expanding fluids would have escaped into the surrounding magma (Murrell and Ismail, 1976a,b; Knapp and Knight, 1977; Nishiyama, 1989; Dutrow, 1990; Dutrow and Norton, 1991). In the Kap Edvard Holm Complex, the predicted result is contamination of the magma with fluids derived ultimately from the meteoric-hydrothermal system that altered the country rocks prior to stoping. Partial dehydration of the metabasalts may also have occurred *prior* to stoping, as a result of metamorphism in a thermal aureole ahead of the advancing pluton, but the eventual formation of pegmatitic hornblende and phlogopite within the xenoliths indicates that pre-stoping dehydration could not have been complete.

Two-pyroxene thermometry has shown that peak temperatures in the xenoliths exceeded the stability limits of hydrous minerals (approx 900°-975°C for $P_{H_2O} \leq 2$ kb; Yoder and Tilley, 1962; Holloway and Burnham, 1972; Spear, 1981; Spulber and Rutherford, 1983; Beard and Lofgren, 1991). Crystallization of pegmatitic hornblende and phlogopite must therefore have taken place only during cooling of the entire pluton, an inference supported by the retrograde replacement of anhydrous hornfels and pegmatitic pyroxene by megacrysts of igneous horn-

blende (fig. 17). Thus the H_2O that was eventually incorporated into pegmatitic minerals was almost certainly sequestered in partial melts during peak metamorphism. One possible mechanism for retaining H_2O during heating can be inferred from the thermal profiles shown in figure 21: the steep temperature gradients within xenoliths suggest that early partial melts produced near the xenolith margins might have absorbed water that was released during breakdown of hydrous minerals in the cooler xenolith interior.

The abundance of hydrous minerals in the pegmatites, coupled with their absence in the hornfelsed residua, suggests that melt production was limited by the availability of H_2O during anatexis. Thus the water that was added to the country rock protoliths during meteoric-hydrothermal alteration was probably a crucial factor influencing xenolith melting.

Mass Transfer Across Gabbro-Xenolith Contacts

The strong depletion of incompatible elements in most of the hornfelses implies that partial melts were expelled from nearly all the xenoliths. There is, however, little chemical evidence for extensive contamination of the gabbros surrounding most xenoliths. In terms of localized effects, contamination with low-^{18}O material produced only minor ^{18}O depletions in the gabbros even within a few centimeters of gabbro-xenolith contacts (figs. 12, 16). This suggests that most of the assimilated material was dispersed into a large volume of magma. Dispersion may have been facilitated by convection of magma or by mobilization of xenoliths after melt extraction. Minor amounts of *in situ* contamination can, however, still be inferred from the spatial association between metabasaltic xenoliths and zones of postcumulus recrystallization in the gabbros.

Additional evidence for minor *in situ* mass transfer between xenoliths and gabbros has been preserved by spatial variations in mineral compositions. These variations reflect *partial* equilibration within a few centimeters of gabbro-xenolith contacts. An example is illustrated in figure 16, which shows compositions of minerals in a traverse through a 4 m-thick xenolith. Plagioclase in the rim of the xenolith is compositionally almost identical to plagioclase in the gabbro, whereas plagioclase toward the center of the xenolith is distinctly more calcic. This suggests that small-scale mass transfer across the contact facilitated equilibration among plagioclase grains. At the same contact, however, olivine and clinopyroxene in the xenolith are more magnesian than in the gabbro, indicating that complete equilibrium was not attained. Similarly, despite signs of minor oxygen isotope exchange (fig. 16), the $\delta^{18}O$ values of pyroxene differ by 5.6 permil across the contact.

The equilibration of plagioclase, but not of mafic minerals, suggests that mass transfer from gabbro to xenolith did not occur simply by bulk infiltration of the xenolith by gabbroic liquid. It must instead have been a selective process. Measurements of chemical diffusion in silicate liquids have shown that alkalis diffuse orders of magnitude more rapidly than

other common cations (Watson, 1982; Watson and Jurewicz, 1984; Baker, 1990; Watson and Baker, 1991), suggesting that equilibration of plagioclase across the contact could have occurred by rapid diffusion of Na without appreciable movement of other components. This would explain the failure of the ferromagnesian minerals to equilibrate simultaneously. Because changes in plagioclase composition must also have involved the redistribution of Ca, Si, and Al (all of which diffuse much more slowly than Na), this explanation would require that other minerals locally supplied or consumed these components as the plagioclase recrystallized, perhaps via reactions such as:

$$\underset{\textit{liquid}}{2\ Na_2O} + \underset{\textit{plagioclase}}{2\ CaAl_2Si_2O_8} + \underset{\textit{orthopyroxene}}{11\ Mg_2Si_2O_6} \Rightarrow$$

$$\underset{\textit{plagioclase}}{4\ NaAlSi_3O_8} + \underset{\textit{clinopyroxene}}{2\ CaMgSi_2O_6} + \underset{\textit{olivine}}{10\ Mg_2SiO_4}$$

in which breakdown of orthopyroxene provides the silica required to replace calcic plagioclase with sodic plagioclase. Interestingly, orthopyroxene is ubiquitous in the xenolith except within a few centimeters of the contact, where it has disappeared and the modal proportions of augite and olivine have increased (table 14). This is qualitatively consistent with the reaction mechanism described above.

Although no other xenoliths have been analyzed in such detail, perusal of table 2 shows that orthopyroxene is absent from all hornfels samples collected within ~20 cm of gabbro-xenolith contacts and is

TABLE 14

*Modal mineralogies (in volume %) of representative samples of xenolith hornfels**

	KEH259A	KEH267A	KEH274A	KEH274B	KEH274D	KEH303G
plagioclase	19.2	27.4	18.3	27.8	24.0	26.2
clinopyroxene	25.0	53.8	27.4	18.0	19.5	59.8
orthopyroxene	49.4	17.2	-	27.0	33.9	-
olivine	-	1.2	51.0	22.2	12.6	9.8
Fe-Ti oxides	5.8	0.4	3.3	4.6	8.8	4.2
hornblende**	0.6	-	-	trace	0.8	-
phlogopite**	-	-	-	-	trace	-
apatite***	-	-	-	0.4	0.4	trace

* Modes were determined by point-counting on thin sections. 500 points were counted for each sample except KEH274A, for which 1500 points were counted. For fractionation calculations, volume per cents were converted to weight per cents using the following specific gravities: plagioclase = 2.7, clinopyroxene = 3.2, orthopyroxene = 3.5, Fe-Ti oxides = 4.9, hornblende = 3.2, apatite = 3.2.

** Hornblende and phologopite are present as intergranular crystals.

*** Apatite is present as sub-millimeter anhedral poikiloblasts, surrounding rounded grains of the major hornfels minerals.

present in all samples collected further from contacts. This suggests that all xenoliths partially equilibrated with the gabbros over distances of several tens of centimeters. It must be emphasized, however, that the xenoliths retained many of their distinctive chemical characteristics even within a few centimeters of their margins, implying that bulk infiltration by gabbroic liquid was minor or negligible. For example, rough mass balance calculations (based on $\delta^{18}O$ values for pyroxene) indicate that the outermost centimeter of xenolith KEH274 contains less than ~15 percent gabbroic material.

Quantitative Constraints on Melting

Modeling the fractionation of trace elements between liquids and residual solids is a well-established technique for quantitative modeling of melt production during anatexis (Shaw, 1970; Arth, 1976; Hanson, 1989). Most trace elements in the Lower Basalts have highly variable concentrations, so the original abundances and ratios in any particular xenolith cannot be known accurately. These elements (for example, Rb, Ba, Sr, Zr, Nb, Cr, Ni) are not very useful for detailed quantitative modeling. The rare earth elements, however, have a narrower range of concentrations and elemental ratios (Gill and others, 1988; Fram, 1994) and can therefore be used to place reasonable quantitative constraints on melting.

Rare-earth element analyses of four samples of xenolith hornfels are given in table 9 and depicted in figure 20. Three of the samples have been strongly depleted in REE relative to the Lower Basalts, which is qualitatively consistent with expulsion of a partial melt. The extent of melting can be quantified using the fractionation equations of Shaw (1970).

Melting has been modeled according to two simple end-member processes: equilibrium fractional melting (in which the liquid is extracted continuously as it is generated) and equilibrium batch melting (in which the liquid is retained until finally being removed in a single batch). During fractional melting, the concentration of an element in the residual solid is described by the relationship

$$\frac{C_s}{C_o} = (1 - F)^{[(1/\overline{D})-1]}$$

where C_s is the concentration in the solid residue, C_o is the concentration in the original rock, F is the cumulative weight fraction of melt, and $\overline{D}$ is the bulk distribution coefficient between liquid and residual solid (≡ concentration in liquid/concentration in solid; Beattie and others, 1993). For batch melting, the corresponding relationship is

$$\frac{C_s}{C_o} = \frac{1}{1 + F[(1/\overline{D}) - 1]}$$

For each xenolith, C_s was assumed to be the whole-rock concentration of the element in the hornfels. Values of C_o were not known precisely due to

the variability of the Lower Basalts, so for the sake of consistency a single metabasaltic country rock was chosen for the protolith in all calculations. The sample with the lowest measured REE concentrations was selected in order to allow estimation of the *minimum* amounts of melting required to produce the inferred REE depletions.

Values of $\overline{D}$ were calculated from mineral modes (table 14) and published mineral/melt partition coefficients (D; table 15). The modal mineralogy of each xenolith during melting was assumed to be that of the xenolith hornfels (that is, modal melting; non-modal melting was not considered, due to lack of adequate constraints). Calculations were performed using two different sets of values for D: one for liquids of dacitic composition and one for liquids of basaltic composition. This was done because actual liquid compositions could not be readily inferred, since fusion of metabasites typically yields dacitic or rhyolitic liquids if the extent of melting is small (Holloway and Burnham, 1972; Helz, 1976; Beard and Lofgren, 1991) but can yield dioritic liquids if the extent of melting reaches tens of percent (Spulber and Rutherford, 1983). Batch and fractional melting calculations were performed for each of the four samples, using the two separate sets of D values. The fraction of melting was varied from 0 to 50 percent, and the calculated results were compared with the measured hornfels compositions. Results are summarized in figures 22 and 23.

For equilibrium batch melting, the xenoliths and model residua had REE patterns of similar shape, with the "basaltic" partition coefficients yielding concentrations that in some cases overlapped the measured concentrations. In contrast, fractional melting models generally yielded poor fits to the measured pattern shapes, with model melting curves always being far too strongly depleted in LREE relative to HREE. Given the uncertainties in model parameters (especially the initial REE concentrations), the reasonably good correspondence for the batch melting models suggests that a process approaching batch melting can account for the general features of the xenolith REE patterns. The inferred non-fractional nature of melting suggests that melts were produced faster than they could be extracted from the solid residua, a result that is perhaps not surprising given the short times required for heating. For samples strongly depleted in rare earth elements, the better fit for basaltic rather than dacitic partition coefficients is consistent with large fractions of melting.

For sample KEH274D, batch melting calculations yielded model restite curves that matched the measured curve at ≤ 5 percent melting (fig. 23). The measured REE pattern was virtually identical to the typical pattern for basalts of the Miki Formation of the Lower Basalts (Fram, 1994), suggesting that little or no melt was extracted from this sample. This inference is supported by other incompatible element concentrations, most of which were within the ranges for the Lower Basalt country rocks (fig. 14).

TABLE 15

Mineral/melt partition coefficients (D) used in partial melting calculations

	Basaltic liquids						
	plag	cpx	opx	ol	Fe-Ti ox**	hb	ap
La	0.089	0.058	0.0067	0	0.003	0.17	3.0
Ce	0.063	0.10	0.0078	0	0.004	0.26	4.4
Sm	0.027	0.45	0.019	0.001	0.007	0.76	6.7
Eu	0.242	0.48	0.022	0.002	0.006	0.88	3.7
Tb	0.019	0.59	0.050	0.005	0.006	0.83	6.0
Yb	0.017	0.58	0.14	0.036	0.018	0.59	3.0
Lu	0.018	0.53	0.18	0.051	0.023	0.51	2.7

	*Dacitic liquids**						
	plag	cpx	opx	ol+	Fe-Ti ox**+	hb	ap
La	0.18	0.18	0.10	0	0.003	0.28	14.5
Ce	0.20	0.30	0.10	0	0.004	0.48	21.1
Sm	0.08	0.98	0.15	0.001	0.007	1.69	46.0
Eu	0.77	0.91	0.15	0.002	0.006	1.71	25.5
Tb	0.05	1.43	0.26	0.005	0.006	2.23	43.9
Yb	0.02	1.11	0.43	0.036	0.018	1.72	15.4
Lu	0.03	1.10	0.54	0.051	0.023	1.63	13.8

plag = plagioclase, cpx = clinopyroxene, opx = orthopyroxene, ol = olivine, Fe-Ti ox = magnetite + ilmenite, hb = hornblende, ap = apatite

* D values for dacitic liquids were compiled mostly from data for porphyritic andesites, which have glasses of roughly dacitic composition.

** Ilmenite and magnetite were not tabulated separately during point counting. Because their D values are similar (Nielsen, Gallahan, and Newberger, 1992), coefficients for magnetite were used for both minerals.

+ Due to the lack of reliable partitioning data for olivine and Fe-Ti oxides in felsic rocks, values for basaltic rocks were used. This approximation has little effect on calculations due to the low D values for these minerals.

SOURCES OF DATA, BASALT: plag: Higuchi and Nagasawa (1969), Schnetzler and Philpotts, 1970, Fujimaki, Tatsumoto, and Aoki (1984); cpx, opx, hb: Irving and Frey (1984); ol, Fe-Ti ox: Nielsen, Gallahan, and Newberger (1992); ap: Watson and Green (1981). *SOURCES OF DATA, DACITE:* plag: Okamoto (1979), Luhr and Carmichael (1980), Fujimaki, Tatsumoto, and Aoki (1984); cpx, opx: Schnetzler and Philpotts (1970), Okamoto (1979), Luhr and Carmichael (1980), Fujimaki, Tatsumoto, and Aoki (1984); hb: Schnetzler and Philpotts (1970), Arth and Barker (1976), Luhr and Carmichael (1980), Fujimaki, Tatsumoto, and Aoki (1984); ap: Fujimaki (1986).

The other xenoliths were strongly depleted in rare earth elements relative to the Lower Basalt country rocks (fig. 20). For sample KEH259A, roughly 30 to 50 percent batch melting (with "basaltic" partition coefficients) accounted reasonably well for the measured REE pattern (fig. 22).

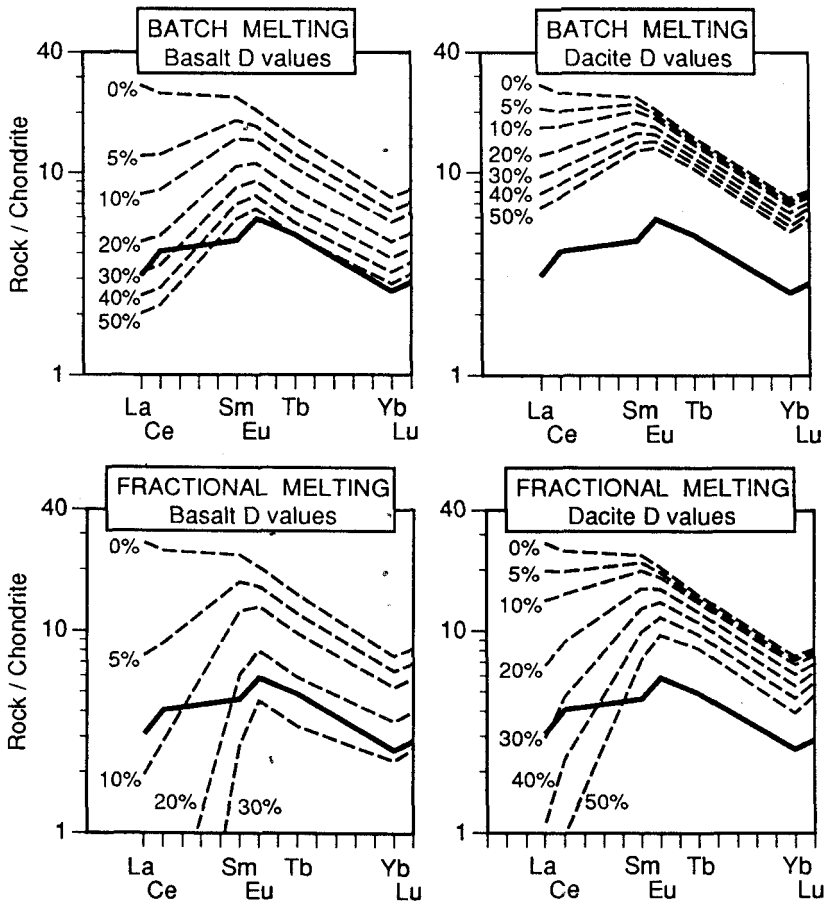

Fig. 22. Results of model melting calculations for xenolith sample KEH259A. Solid lines are measured REE concentrations; dashed lines are calculated concentrations in solid residua after various fractions of melting. Curves labeled "0%" are model initial concentrations, equivalent to Lower Basalt sample 1133 (table 1).

At these fractions of melting, the liquid would probably have been dioritic or perhaps tonalitic (Spulber and Rutherford, 1983; Beard and Lofgren, 1991; Sisson and Grove, 1993). For the other two samples (KEH267 and KEH303G) single-step equilibrium melting models could not account for the extensive depletions of HREE (fig. 23).

At least two plausible hypotheses can explain the anomalously low REE concentrations in these last two samples. One is that the xenoliths were not derived from the Lower Basalts but are instead pieces of the fine-grained gabbros marginal to the complex. In this case, the failure of the melting models could simply reflect an inappropriate choice of

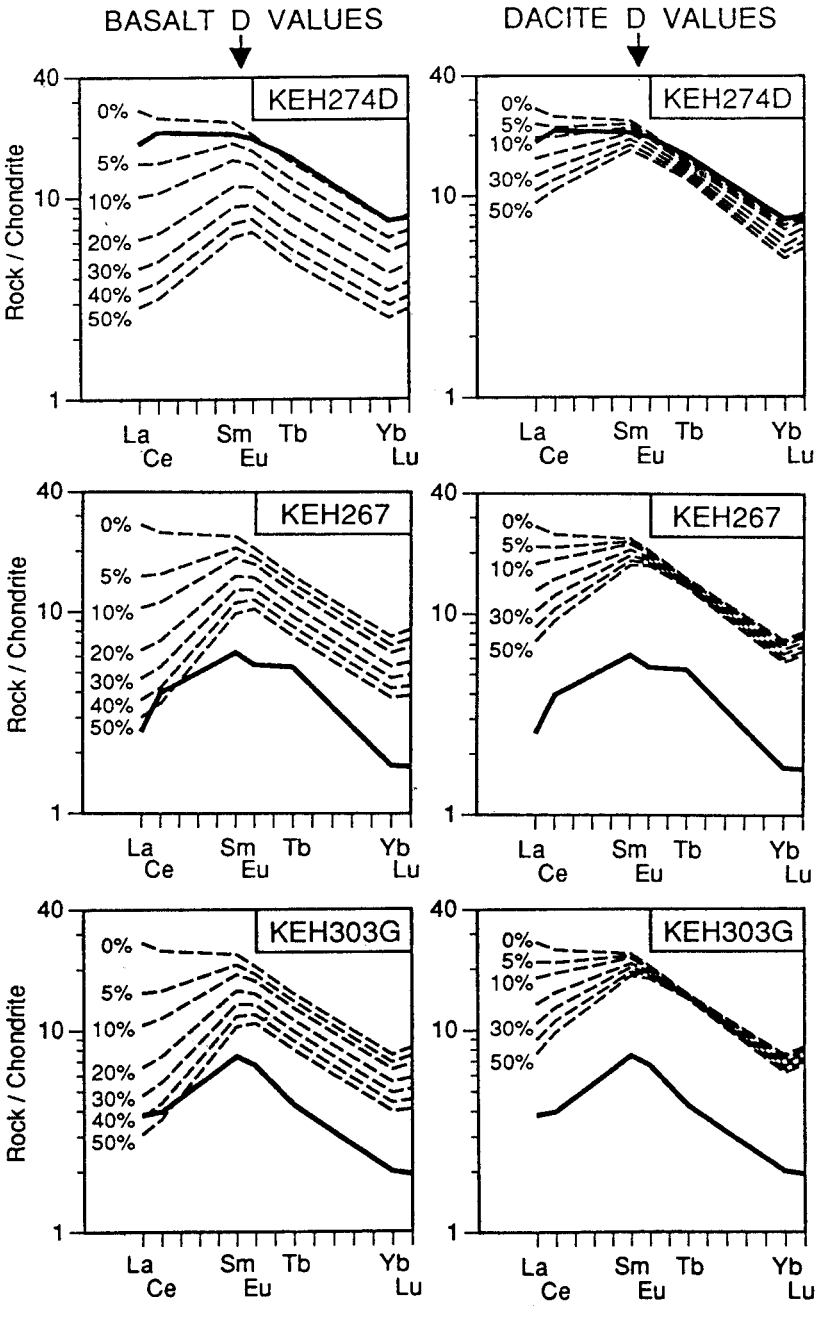

Fig. 23. Results of model batch melting calculations for metabasalt xenolith samples KEH274D, KEH267, and KEH303G. See figure 22 for details.

protolith. A more likely possibility, based on mineralogic observations, is that the xenoliths *are* fragments of the Lower Basalts but that the modal abundances of minerals in the hornfels do *not* reflect the modal abundances at the time of melting. As previously noted, a traverse through one xenolith (KEH274A-D) showed that clinopyroxene was most abundant near the margin, where it apparently formed at the expense of orthopyroxene during partial equilibration between hornfels and host gabbro. If this equilibration took place *after* the main episode of melting and melt extraction, then the proportion of clinopyroxene *during* melting would have been less than the proportion ultimately preserved. Of the abundant hornfels minerals, clinopyroxene is by far the richest in REE (table 15). Overestimating its abundance during melting would therefore yield predicted residual REE concentrations that would be much too high. This appears to be a good explanation for the disparity between predicted and measured REE concentrations in the two problematical samples (KEH267 and KEH303G): both are from near the margins of xenoliths (table 2), both contain no orthopyroxene but contain 50 to 60 percent clinopyroxene (table 14), and both have REE patterns with shapes (but not magnitudes) that are consistent with a batch melting model in which REE concentration is controlled largely by partitioning into clinopyroxene (fig. 23). In addition, both have $\delta^{18}O$ values that are higher than those of most other xenoliths, suggestive of minor oxygen exchange with the gabbroic magma.

Rare-earth element concentrations in all the analyzed xenoliths therefore appear to be consistent with a process of near-equilibrium partial melting and melt extraction via a process that more closely approached batch melting than fractional melting. The similarity of rare earth element concentrations in the three REE-depleted xenoliths suggests that they underwent grossly similar amounts of melting (at least 30-50 percent, as calculated for sample KEH259A; fig. 22). This must be considered a crude estimate for the orthopyroxene-free samples, which may have undergone substantial changes in modal mineralogy *after* melt extraction and therefore cannot be modeled quantitatively. The concentrations of other elements are generally consistent with such large extents of melting, but meaningful quantitative assessments are hampered by the compositional variability of the protoliths (a severe problem for compatible elements), the extreme sensitivity of the calculations to minor errors at large fractions of melting (a major problem for highly incompatible elements), and the uncertainties in partition coefficients.

Melt Segregation

Although melts have clearly been extracted from most xenoliths, the mechanisms of melt segregation are ambiguous. Many xenoliths appear to have been flattened, suggesting that melt extraction could have been facilitated by deformation. Evidence for deformation includes the flattening of amygdules and the development of foliations parallel to the direction of xenolith elongation (fig. 18). Deformation might have been

caused by compaction under the weight of overlying cumulates (Irvine, 1980; Sparks and others, 1985) or by shearing due to the flow of surrounding cumulates or magma (Green and Kenyon, 1992). The batch melting process inferred from trace element modeling implies that melts were generated faster than they could be extracted from the solid residua.

The entrapment of anatectic liquids within xenoliths indicates that melt extraction was not always complete. One interesting example is xenolith KEH274. The center of this xenolith (fig. 2A) contains many small pods of pegmatite enriched in incompatible elements, but trace element modeling has demonstrated that very little melt was extracted from the nearby hornfels. This suggests that small pools of liquid became trapped in zones where the hornfels did not reach the critical melt percentage required for large-scale liquid coalescence and migration. In xenoliths that underwent extensive and pervasive melt extraction *prior* to the trapping of the latest melt fractions, the trapped liquids precipitated relatively calcic plagioclase because the earliest melt fractions had already been withdrawn (for example samples KEH259 and KEH263, table 13).

Effects on the Host Gabbros

The association of metabasaltic xenoliths with zones of postcumulus recrystallization in the host gabbros suggests that crustal contamination affected phase relationships in the crystallizing pluton. On the basis of their mineralogical, textural, and geometrical characteristics, the postcumulus rocks are most easily interpreted as products of interaction between layered gabbroic cumulates and the hydrous liquids or fluids that were expelled from xenoliths. The formation of peridotite from gabbro requires extensive resorption of plagioclase; this can be attributed most simply to an influx of H_2O, which destabilizes plagioclase relative to mafic minerals (Helz, 1976; Spulber and Rutherford, 1983; Beard and Lofgren, 1991; Sisson and Grove, 1993). Contamination with hydrous liquids can also account for the localized formation of coarse-grained or pegmatitic gabbros, as high H_2O concentrations in gabbros can cause textural coarsening (Larsen and Brooks, 1994). The abundance of late-magmatic hornblende and biotite in the postcumulus rocks provides further evidence for the involvement of a hydrous liquid in the recrystallization process. On the basis of these observations and inferences, we hypothesize that water-rich fluids or melts were expelled from the xenoliths and infiltrated the partially solidified cumulates, where they resorbed plagioclase and left ultramafic residua; the plagioclase-rich liquids then segregated, mixed with nearby gabbroic cumulates, and crystallized as bodies of coarse-grained to pegmatitic gabbro. In places, contamination probably resulted in the resorption and in situ recrystallization of cumulates, forming postcumulus gabbros such as those encrusting some xenoliths (fig. 9).

The oxygen isotope compositions of the postcumulus rocks were affected only slightly by contamination (fig. 12), implying that recrystalli-

zation was caused by relatively small amounts of highly reactive contaminant. The hydrous fluids or melts involved in the recrystallization process were therefore probably only a small fraction of the entire mass assimilated.

The branching shapes of the small periodotitic bodies (fig. 10) reveal the irregular pathways along which the contaminating liquids infiltrated the partially solidified cumulus mushes. In mineralogically zoned peridotites such as those shown in figure 10, the destabilization inward first of plagioclase and then of pyroxene can probably be attributed to progressively higher H_2O activities toward the centers of permeable intracumulus conduits. The selective development of replacement bodies along planes of foliation suggests that permeability was highest in this direction. However, the migrating liquids were probably buoyant due to their high H_2O contents and therefore also percolated upward to produce local discordancies.

The operation of such processes on a large scale is inferred from the development of peridotite and coarsely recrystallized gabbro as semiconformable layers hundreds of meters in length. As described earlier, these larger bodies are mineralogically and texturally similar to the smaller postcumulus bodies shown in figures 9 and 10 and form the same bimodal association of rock types. Like the smaller bodies, they are spatially associated with xenoliths and are locally discordant to the overlying layered gabbros (fig. 11). The sequence of events by which these major features formed is uncertain, but one possibility is that cumulates were contaminated during devolatilization or melting of xenoliths on the floor of the intrusion. In this case the xenoliths must have been buried rapidly enough for hydrous contaminants to become trapped in the growing cumulus pile. Alternatively, the xenoliths may have devolatilized while enveloped in a zone of crystallization along the walls of the pluton, with the xenoliths and their anomalously mafic host cumulates (the "mafic macrolayers," in which plagioclase crystallization was suppressed) having been deposited together during slumping of contaminated mushes onto the chamber floor (Irvine, 1987). In either case, the development of such major features suggests that partial assimilation of hydrous mafic xenoliths can potentially affect the large-scale petrologic evolution of large intrusions.

Conclusion

We have demonstrated that metabasaltic xenoliths in the Kap Edvard Holm Complex were derived from hydrothermally altered and hydrated basaltic country rocks and that they underwent dehydration, partial melting, and hornfelsic recrystallization at temperatures $\geq 1050°C$. We have presented evidence for the generation of hydrous fluids and melts and for the destabilization of cumulus minerals in the host gabbros as a result of contamination with these liquids. Because small amounts of H_2O can have relatively large effects on phase relationships in mafic systems, dispersion of hydrous contaminants into basaltic magmas can

substantially alter liquid lines of descent while leaving few obvious signs of contamination (Michael and Schilling, 1989; Cornell, Taylor, and Perfit, 1989; Taylor, Cornell, and Perfit, 1992). Given the widespread presence of metabasaltic and metagabbroic xenoliths in mafic plutons, we suggest that contamination with hydrous material derived from altered mafic xenoliths may commonly affect the petrogenetic evolution of mafic magmas.

ACKNOWLEDGMENTS

This research was conducted while the first author was a graduate student at Stanford University. Logistical support was provided by John Arnason, Richard Nevle, Peggy O'Day, Hreinn Skagfjord, Platinova Resources Ltd., and the Dihedral Exploration Company. Technical advice and support were provided by Greg Arehart and Torsten Venneman in the stable isotope laboratory and by Joel Sparks in the XRF laboratory. Help with XRF sample preparation and analysis was provided by Rónadh Cox and Tamara Lowe. The Sr isotope data were collected by James Wright at Rice University. Access to unpublished chemical data for the Lower Basalts were generously given by C. Kent Brooks, Miranda Fram, Paul Holm, Charles Lesher, and Troels Nielsen. Helpful reviews were provided by Konrad Krauskopf, Charles Lesher, Gail Mahood, Jonathan Stebbins, and an anonymous referee. Financial support was provided by the National Science Foundation (grants NSF-EAR-8803754, NSF-EAR-9004007 and NSF-EAR-9220431, all to D.K. Bird, and NSF-EAR-9205314 to J.R. O'Neil), the Richard and Frances Jahns Fund, the Geological Society of America, the Chevron Corporation, the Shell Corporation, and the McGee Trust.

REFERENCES

Abbott, D., and Deer, W. A., 1972, Geological investigations in East Greenland, Part X: the gabbro cumulates of the Kap Edvard Holm Lower Layered Series: Meddelelser om Grønland, v. 190, number 6.

Andersen, D. J., Lindsley, D. H., and Davidson, P. M., 1993, QUILF: A PASCAL program to assess equilibria among Fe-Mg-Ti oxides, pyroxenes, olivine, and quartz: Computers and Geosciences, v. 19, p. 1333–1350.

Arth, J. G., 1976, Behavior of trace elements during magmatic processes—a summary of theoretical models and their applications: United States Geological Survey Journal of Research, v. 4, p. 41–47.

Arth, J. G., and Barker, F., 1976, Rare-earth partitioning between hornblende and dacitic liquid and implications for the genesis of trondhjemitic-tonalitic magmas: Geology, v. 4, p. 534–536.

Ashworth, J. R., and McLellan, E. L., 1985, Testures, *in* Ashworth, J. R. editor, Migmatites: Glasgow, Blackie and Son, p. 180–203.

Baker, D. R., 1990, Chemical interdiffusion of dacite and rhyolite: anhydrous measurements at 1 atm and 10 kbar, application of transition state theory, and diffusion in zoned magma chambers: Contributions to Mineralogy and Petrology, v. 104, p. 407–423.

Beard, J. S., and Lofgren, G. E., 1991, Dehydration melting and water-saturated melting of basaltic and andesitic greenstones and amphibolites at 1, 3, and 6.9 kb: Journal of Petrology, v. 32, p. 365–401.

Beattie, P., Drake, M., Jones, W., Leeman, W., Longhi, J., McKay, G., Nielsen, R., Palme, H., Shaw, D., Takahashi, E., and Watson, B., 1993, Terminology for trace element partitioning: Geochimica et Cosmochimica Acta, v. 57, p. 1605–1606.

Bédard, J. H., and Hébert, R., 1992, Ophiolite analogue for the oceanic crust: EOS, v. 73, p. 358.

Bernstein, S., Rosing, M. T., Brooks, C. K., and Bird, D. K., 1992, An ocean-ridge type magma chamber at a passive volcanic, continental margin: the Kap Edvard Holm layered gabbro complex, East Greenland: Geological Magazine, v. 129, p. 437–456.

Bird, D. K., Manning, C. E., and Rose, N. M., 1988, Mineralogic and isotopic constraints on the regional hydrology of the Skaergaard magma-hydrothermal system, East Greenland: Geological Society of America Abstracts with Programs, v. 20, p. A344.

Bird, D. K., Rosing, M. T., Manning, C. E., and Rose, N. M., 1985, Geologic field studies of the Miki Fjord Area, East Greenland: Bulletin of the Geological Society of Denmark, v. 34, p. 219–235.

Bott, M. H. P., 1987, The continental margin of central East Greenland in relation to North Atlantic plate tectonic evolution: Journal of the Geological Society of London, v. 144, p. 561–568.

Bottinga, Y., and Javoy, M., 1975, Oxygen isotope partitioning among the minerals in igneous and metamorphic rocks: Reviews of Geophysics and Space Physics, v. 13, p. 401–418.

Brandriss, M. E., ms 1993, Assimilation of metabasalt xenoliths and postcumulus metasomatism of gabbros in the Kap Edvard Holm Complex, East Greenland: Ph.D. thesis, Stanford University, Palo Alto, California, 277 p.

Brandriss, M. E., Bird, D. K., and O'Neil, J. R., 1992, Dependence of hydrotheral alteration on rock texture and microporosity in mafic crystalline rocks, *in* Kharaka, Y. K., and Maest, A. S., editors, Water-Rock Interaction, Proceedings of the 7th international symposium on water-rock interaction, volume 2: moderate and high temperature environments: Rotterdam, A. A. Balkema, p. 1477–1480.

Brandriss, M. E., Nevle, R. J., Bird, D. K., and O'Neil, J. R., 1995, Imprint of meteoric water on the stable isotope compositions of igneous and secondary minerals, Kap Edvard Holm Complex, East Greenland: Contributions to Mineralogy and Petrology, v. 121, p. 74–86.

Brooks, C. K., and Nielsen, T. F. D., 1982a, The Phanerozoic development of the Kangerdlugssuaq area, East Greenland: Meddelelser om Grønland, Geoscience 9.

———— 1982b, The E Greenland continental margin: a transition between oceanic and continental magmatism: Journal of the Geological Society of London, v. 139, p. 265–275.

Brooks, C. K., Nielsen, T. F. D., and Petersen, T. S., 1976, The Blosseville coast basalts of East Greenland: composition and temporal variation: Contributions to Mineralogy and Petrology, v. 58, p. 279–292.

Carslaw, H. S., and Jaeger, J. C., 1959, Conduction of heat in solids, 2nd edition: Oxford, Clarendon Press, 510 p.

Clayton, R. N., and Mayeda, T. K., 1963, The use of bromine pentafluoride in the extraction of oxygen from oxides and silicates for isotopic analysis. Geochimica et Cosmochimica Acta, v. 27, p. 43–52.

Clemens, J. D., and Vielzeuf, D., 1987, Constraints on melting and magma production in the crust. Earth and Planetary Science Letters, v. 86, p. 287–306.

Cornell, W. C., Taylor, B. E., and Perfit, M. R., 1989, Basalt to andesite, eastern Galapagos Rift: stable isotope, volatile, and halogen tracers and AFC processes in spreading center magmas: New Mexico Bureau of Mines and Mineral Resources Bulletin, v. 131, p. 61.

Criss, R. E., Gregory, R. T., and Taylor, H. P. Jr., 1987, Kinetic theory of oxygen isotope exchange between minerals and water: Geochimica et Cosmochimica Acta, v. 51, p. 1099–1108.

Cullers, R., Chaudhuri, S., Kilbane, N., and Koch, R., 1979, Rare-earths in size fractions and sedimentary rocks of Pennsylvanian-Permian age from the mid-continent of the U.S.A.: Geochimica et Cosmochimica Acta, v. 43, p. 1285–1301.

Davidson, P. M., and Lindsley, D. H., 1989, Thermodynamic analysis of pyroxene-olivine-quartz equilibria in the system CaO-MgO-FeO-SiO_2: American Mineralogist, v. 74, p. 18–30.

Deer, W. A., and Abbott, D., 1965, Clinopyroxenes of the gabbro cumulates of the Kap Edvard Holm complex, East Greenland: Mineralogical Magazine, Tilley volume, p. 177–193.

Dixon, S., and Rutherford, M., 1979, Plagiogranites as late-stage immiscible liquids in ophiolite and mid-ocean ridge suites: an experimental study: Earth and Planetary Science Letters, v. 45, p. 45–60.

Dutrow, B., 1990, Pore fluid pressure and the timing of fluid-mineral interaction in contact metamorphic settings: a preliminary analysis: Geological Society of America Abstracts with Programs, v. 22, p. 213–214.

Dutrow, B., and Norton, D., 1991, The generation of a percolation network: fluid pressure, fracture propagation and fluid flow: Geological Society of America Abstracts with Programs, v. 23, p. 49.

Elsdon, R., 1969, The structure and intrusive mechanism of the Kap Edvard Holm layered gabbro complex, East Greenland: Geological Magazine, v. 106, p. 46–56.

———— 1971, Crystallization history of the Upper Layered Series, Kap Edvard Holm, East Greenland: Journal of Petrology, v. 12, p. 499–521.

Fehlhaber, K., and Bird, D. K., 1991, Oxygen-isotope exchange and mineral alteration in gabbros of the Lower Layered Series, Kap Edvard Holm Complex, East Greenland: Geology, 1 v. 9, p. 819–822.

Forester, R. W., and Taylor, H. P. Jr., 1977, $^{18}O/^{16}O$, D/H, and $^{13}C/^{12}C$ studies of the Tertiary igneous complex of Skye, Scotland: American Journal of Science, v. 277, p. 137–177.

Fram, M. S., ms 1994, Petrogenesis of the early Tertiary flood basalts of the East Greenland continental margin: Ph.D. thesis, Columbia University, Palisades, New York, 268 p.

Fujimaki, H., 1986, Partition coefficients of Hf, Zr, and REE between zircon, apatite, and liquid: Contributions to Mineralogy and Petrology, v. 94, p. 42–45.

Fujimaki, H., Tatsumoto, M., and Aoki, K., 1984, Partition coefficients of Hf, Zr, and REE between phenocrysts and groundmasses, *in* Proceedings of the 14th Lunar and Planetary Science Conference, Part 2: Journal of Geophysical Research, v. 89, supplement, p. B662–B672.

Furlong, K. P., and Myers, J. D., 1985, Thermal-mechanical modeling of the role of thermal stresses and stoping in magma contamination: Journal of Volcanology and Geothermal Research, v. 24, p. 179–191.

Gill, R. C. O., Nielsen, T. F. D., Brooks, C. K., and Ingram, G. A., 1988, Tertiary volcanism in the Kangerdlugssuaq region, E Greenland: trace-element geochemistry of the Lower Basalts and tholeiitic dyke swarms, *in* Morton, A. C., and Parsons, L. M., editors, Early Tertiary volcanism and the opening of the NE Atlantic: Geological Society Special Publication no. 39, p. 161–179.

Gordon, G. E., Randle, K., Goles, G., Corliss, J., Beeson, M. H., and Olsey, S. S., 1968, Instrumental neutron activation analysis of standard rocks with high-resolution gamma ray detectors: Geochimica et Cosmochimica Acta, v. 32, p. 369–396.

Green, N. L., and Kenyon, P. M., 1992, Crustal contamination by disaggregation of partially fused xenolith margins: EOS, v. 73, p. 353.

Gregory, R. T., Criss, R. E., and Taylor, H. P. Jr., 1989, Oxygen isotope exchange kinetics of mineral pairs in closed and open systems: applications to problems of hydrothermal alteration of igneous rocks and Precambrian iron formations: Chemical Geology, v. 75, p. 1–42.

Gregory, R. T., and Taylor, H. P. Jr., 1981, An oxygen isotope profile in a section of Cretaceous oceanic crust, Samail Ophiolite, Oman: evidence for $\delta^{18}O$ buffering of the oceans by deep, >5 km, seawater-hydrothermal circulation at mid-ocean ridges: Journal of Geophysical Research, v. 86, p. 2737–2755.

Habekost, E. M., and Wilson, J. R., 1989, Raft-like metabasalt inclusions in the Fongenhyllingen layered intrusive complex, Norway, and their implications for magma chamber evolution: Journal of Petrology, v. 30, p. 1415–1441.

Hanson, G. N., 1989, An approach to trace element modeling using a simple igneous system as an example, *in* Lipin, B. R., and McKay, G. A., editors, Geochemistry and mineralogy of rare earth elements: Washington D.C., Mineralogical Society of America, p. 79–97.

Hattori, K., and Muehlenbachs, K., 1982, Oxygen isotope ratios of the Icelandic crust: Journal of Geophysical Research, v. 87, p. 6559–6565.

Helz, R. T., 1976, Phase relations of basalts in their melting ranges at P_{H_2O} = 5 kb. Part II. Melt compositions: Journal of Petrology, v. 17, p. 139–193.

Henderson, P., 1982, Inorganic geochemistry: Oxford, Pergamon Press, 353 p.

Higuchi, H., and Nagasawa, H., 1969, Partition of trace elements between rock-forming minerals and the host volcanic rocks: Earth and Planetary Science Letters, v. 7, p. 281–287.

Holloway, J. R., and Burnham, C. W., 1972, Melting relations of basalt with equilibrium water pressure less than total pressure: Journal of Petrology, v. 13, p. 1–29.

Holm, P. M., 1988, Nd, Sr and Pb isotope geochemistry of the Lower Lavas, E Greenland Tertiary Igneous Province, *in* Morton, A. C., and Parsons, L. M., editors, Early Tertiary volcanism and the opening of the NE Atlantic: Geological Society Special Publication No. 39, p. 181–195.

Irvine, T. N., 1980, Magmatic infiltration metasomatism, double-diffusive fractional crystallization, and adcumulus growth in the Muskox Intrusion and other layered intrusions, *in* Hargraves, R. B., editor, Physics of magmatic processes: Princeton, New Jersey, Princeton University Press, p. 325–383.

———— 1987, Layering and related structures in the Duke Island and Skaergaard intrusions: similarities, differences, and origins, *in* Parsons, I., editor, Origins of Igneous Layering: Dordrecht, D. Reidel, p. 185–245.

Irving, A. J., and Frey, F. A., 1984, Trace element abundances in megacrysts and their host basalts: constraints on partition coefficients and megacryst genesis: Geochimica et Cosmochimica Acta, v. 48, p. 1201–1221.

Ito, E., and Clayton, R. N., 1983, Submarine metamorphism of gabbros form the Mid-Cayman Rise: an oxygen isotope study: Geochimica et Cosmochimica Acta, v. 47, p. 535–546.

Jacobs, J. W., Korotov, R. L., Blanchard, D. P., and Haskin, L. A., 1977, A well-tested procedure for instrumental neutron activation analysis of silicate rocks and minerals: Journal of Radioanalytical Chemistry, v. 40, p. 93–114.

Johannes, W., 1985, The significance of experimental studies for the formation of migmatites, *in* Ashworth, J. R., editor, Migmatites: Glasgow, Blackie and Son, p. 36–85.

Kays, M. A., Goles, G. G., and Grover, T. W., 1989, The Precambrian sequence bordering the Skaergaard intrusion: Journal of Petrology, v. 30, p. 321–361.

Kempton, P. D., Hawkesworth, C. J., and Fowler, M., 1991, Geochemistry and isotopic composition of gabbros from Layer 3 of the Indian Ocean crust, Hole 735B, *in* Von Herzen, R. P., and Robinson, P. T., editors, Proceedings of the Ocean Drilling Program, Scientific Results: v. 188, p. 153–180.

Knapp, R. B., and Knight, J. E., 1977, Differential thermal expansion of pore fluids: fracture propagation and microearthquake production in hot pluton environments: Journal of Geophysical Research, v. 82, p. 2115–2122.

Kyser, T. K., 1986, Stable isotope variations in the mantle, *in* Valley, J. W., Taylor, H. P. Jr., and O'Neil, J. R., editors, Stable isotopes in high temperature geological processes: Washington D.C., Mineralogical Society of America, p. 141–164.

Larsen, R. B., and Brooks, C. K., 1994, Origin and evolution of gabbroic pegmatites in the Skaergaard Intrusion, East Greenland: Journal of Petrology, v. 35, p. 1651–1679.

Liou, J. G., Kuniyoshi, S., and Ito, K., 1974, Experimental studies of the phase relations between greenschist and amphibolite in a basaltic system: American Journal of Science, v. 274, p. 613–632.

Luhr, J. F., and Carmichael, I. S. E., 1980, The Colima Volcanic Complex, Mexico: I. Post-caldera andesites from Volcán Colima: Contributions to Mineralogy and Petrology, v. 71, p. 343–372.

Malpas, J., Brace, T., and Dunsworth, S. M., 1989, Structural and petrologic relationships of the CY-4 drill hole of the Cyprus Crustal Study Project, *in* Gibson, I. L., Malpas, J., Robinson, P. T., and Xenophontos, C., editors, Cyprus Crustal Study Project: Initial Report, Hole CY-4: Geological Survey of Canada Paper 88-9, p. 39–67.

Manning, C. E., and Bird, D. K., 1991, Porosity evolution and fluid flow in the basalts of the Skaergaard magma-hydrothermal system, East Greenland: American Journal of Science, v. 291, p. 201–257.

———— 1995, Porosity, permeability, and basalt metamorphism, *in* Day, H., and Schiffman, P., editors., The transition from basalt to metabasalt: Geological Society of America Special Paper 296, p. 123–140.

Manning, C. E., Ingebritsen, S. E., and Bird, D. K., 1993, Missing mineral zones in contact metamorphosed basalts: American Journal of Science, v. 293, p. 894–938.

Marsh, B. D., 1982, On the mechanics of igneous diapirism, stoping, and zone melting: American Journal of Science, v. 282, p. 808–855.

Matthews, A., Goldsmith, J. R., and Clayton, R. N., 1983, Oxygen isotope fractionations involving pyroxenes: the calibration of mineral-pair geothermometers: Geochimica et Cosmochimica Acta, v. 47, p. 631–644.

McLellan, E. L., 1983, Contrasting textures in metamorphic and anatectic migmatites: an example from the Scottish Caledonides: Journal of Metamorphic Geology, v. 1, p. 241–262.

Michael, P. J., and Schilling, J.-G., 1989, Chlorine in mid-ocean ridge magmas: Evidence for assimilation of seawater-influenced components: Geochimica et Cosmochimica Acta, v. 53, p. 3131–3143.

Misch, P., 1968, Plagioclase compositions and non-anatectic origin of migmatitic gneisses in Northern Cascade Mountains of Washington State: Contributions to Mineralogy and Petrology, v. 17, p. 1–70.

Murrell, S. A. F., and Ismail, I. A. H., 1976a, The effect of decomposition of hydrous minerals on the mechanical properties of rocks at high pressures and temperatures: Tectonophysics, v. 31, p. 207–258.

———— 1976b, The effect of temperature on the strength at high confining pressure of granodiorite containing free and chemically-bound water: Contributions to Mineralogy and Petrology, v. 55, p. 317–330.

Nevle, R. J., Brandriss, M. E., Bird, D. K., McWilliams, M. O., and O'Neil, J. R., 1994, Tertiary plutons monitor climate change in East Greenland: Geology, v. 22, p. 775–778.

Nielsen, R. L., 1992, BIGD.FOR; Fortran program to calculate trace-element partition coefficients for natural mafic and intermediate composition magmas: Computers and Geosciences, v. 18, p. 773–788.

Nielsen, R. L, Gallahan, W. E., and Newberger, F., 1992, Experimentally determined mineral-melt partition coefficients for Sc, Y and REE for olivine, orthopyroxene, pigeonite, magnetite and ilmenite: Contributions to Mineralogy and Petrology, v. 110, p. 488–499.

Nielsen, T. F. D., and Brooks, C. K., 1981, The E Greenland rifted continental margin: an examination of the coastal flexure: Journal of the Geological Society of London, v. 138, p. 559–568.

Nielsen, T. F. D., Soper, N. J., Brooks, C. K., Faller, A. M., Higgins, A. C., and Matthews, D. W., 1981, The pre-basaltic sediments and the Lower Basalts at Kangerdlugssuaq, East Greenland: their stratigraphy, lithology, palaeomagnetism and petrology: Meddelelser om Grønland, Geoscience 6.

Nishiyama, T., 1989, Kinetics of hydrofracturing and metamorphic veining: Geology, v. 17, p. 1068–1071.

Noble, R. H., Macintyre, R. M., and Brown, P. E., 1988, Age constraints on Atlantic evolution: timing of magmatic activity along the E Greenland continental margin, *in* Morton, A. C., and Parsons, L. M., editors, Early Tertiary volcanism and the opening of the NE Atlantic: Geological Society Special Publication. no. 39, p. 201–214.

Norrish, K., and Chappel, B. W., 1977, X-ray fluorescence spectrometry, *in* Zussmann, J., editor, Physical methods in determinative mineralogy: New York, Academic Press, p. 201–272.

Norrish, K., and Hutton, J. T., 1969, An accurate x-ray spectrographic method for the analysis of a wide range of geological samples: Geochimica et Cosmochimica Acta, v. 334, p. 31–453.

Okamoto, K., 1979, Geochemical study on magmatic differentiation of Asama volcano, central Japan: Journal of the Geological Society of Japan, v. 85, p. 525–535.

Pankhurst, R. J., Beckinsale, R. D., and Brooks, C. K., 1976, Strontium and oxygen isotopic evidence relating to the petrogenesis of the Kangerdlugssuaq alkaline intrusion, East Greenland: Contributions to Mineralogy and Petrology, v. 54, p. 17–42.

Pedersen, R. B., 1986, The nature and significance of magma chamber margins in ophiolites: examples from the Norwegian Caledonides: Earth and Planetary Science Letters, v. 77, p. 100–112.

Petrunin, G. I., Yurchak, R. I., and Tkach, G. F., 1971, Temperature conductivity of basalts at temperatures from 300 to 1200°K: Physics of the Solid Earth, v. 7, p. 126–127.

Rose, N. M., ms, 1989, Geochemistry of hydrothermal metasomatism in basaltic systems, Ph.D. thesis, Stanford University, Palo Alto, California, 232 p.

Rosing, M. T., and Lesher, C. E., 1992, P-T conditions for metabasalt transformation in the roof pendant of the Miki Fjord Macrodike from the occurrence of spinel, cordierite, and quartz: EOS, v. 73, p. 640.

Schnetzler, C. C., and Philpotts, J. A., 1970, Partition coefficients of rare earth elements and barium between igneous matrix minerals and rock forming mineral phenocrysts—II: Geochimica et Cosmochimica Acta, v. 34, p. 331–340.

Shaw, D. M., 1970, Trace element fractionation during anatexis: Geochimica et Cosmochimica Acta, v. 34, p. 237–243.

Sigmarsson, O., Condomines, M., and Fourcade, S., 1992, Mantle and crustal contribution in the genesis of Recent basalts from off-rift zones in Iceland: constraints from Th, Sr, and O isotopes: Earth and Planetary Science Letters, v. 110, p. 149–162.

Sisson, T. W., and Grove, T. L., 1993, Experimental investigations of the role of H_2O in calc-alkaline differentiation and subduction zone magmatism: Contributions to Mineralogy and Petrology, v. 113, p. 143–166.

Soper, N. J., Higgins, A. C., Downie, C., Matthews, D. W., and Brown, P. E., 1976, Late Cretaceous-early Tertiary stratigraphy of the Kangerdlugssuaq area, East Greenland and the age of opening of the North Atlantic: Journal of the Geological Society of London, v. 132, p. 85–104.

Sparks, R. S. J., Huppert, H. E., Kerr, R. C., McKenzie, D. P., and Tait, S. R., 1985, Postcumulus processes in layered intrusions: Geological Magazine, v. 122, p. 555–568.

Spear, F. S., 1981, An experimental study of hornblende stability and compositional variability in amphibolite: American Journal of Science, v. 281, p. 697–734.

Spulber, S. D., and Rutherford, M. J. 1983, The origin of rhyolite and plagiogranite in oceanic crust: an experimental study: Journal of Petrology, v. 24, p. 1–25.

Stakes, D. S., 1991, Oxygen and hydrogen isotope compositions of oceanic plutonic rocks: High-temperature deformation and metamorphism of oceanic layer 3, *in* Taylor, H. P. Jr., O'Neil, J. R., and Kaplan, I. R., editors, Stable isotope geochemistry: a tribute to Samuel Epstein: San Antonio, Texas, The Geochemical Society, p. 77–90.

Stakes, D. S., Taylor, H. P. Jr., and Fisher, R. L., 1984, Oxygen-isotope and geochemical characterization of hydrothermal alteration in ophiolite complexes and modern oceanic crust, *in* Gass, I. G., Lippard, S. J., and Shelton, A. W., editors, Ophiolites and oceanic lithosphere: Oxford, Blackwell Scientific Publications, p. 199–214.

Stakes, D. S., Mevel, C., Cannat, M., and Chaput, T., 1991, Metamorphic stratigraphy of Hole 735B, *in* Von Herzen, R. P., and Robinson, P. T., editors, Proceedings of the Ocean Drilling Program, Scientific Results: v. 188, p. 153–180.

Steinthórsson, S., Oskarsson, N., Arnórsson, S., and Gunnlaugsson, E., 1987, Metasomatism in Iceland: hydrothermal alteration and remelting of oceanic crust, *in* Helgeson, H. C., editor, Chemical transport in metasomatic processes: Dordrecht, Reidel, p. 355–387.

Stewart, B. W., and DePaolo, D. J., 1990, Isotopic studies of processes in mafic magma chambers: II. The Skaergaard intrusion, East Greenland: Contributions to Mineralogy and Petrology, v. 104, p. 125–141.

Taylor, B. E., Cornell, W. C., and Perfit, M. R., 1992, The volatile history of the basalt to andesite transition, Eastern Galapagos Rift, 85°W: AFC processes in spreading center magmas: EOS, v. 73, p. 349.

Taylor, H. P. Jr., 1974, The application of oxygen and hydrogen isotope studies to problems of hydrothermal alteration and ore deposition: Economic Geology, v. 69, p. 843–883.

Taylor, H. P. Jr., and Forester, R. W., 1979, An oxygen and hydrogen isotope study of the Skaergaard intrusion and its country rocks: a description of a 55 m.y. old fossil hydrothermal system: Journal of Petrology, v. 20, p. 355–419.

Taylor, H. P. Jr., and Sheppard, S. M. F., 1986, Igenous rocks: I. Processes of isotopic fractionation and isotope systematics, *in* Valley, J. W., Taylor, H. P. Jr., and O'Neil, J. R., editors, Stable isotopes in high temperature geological processes: Washington D.C., Mineralogical Society of America, p. 227–271.

Tegner, C., Wilson, J. R., and Brooks, C. K., 1993, Intraplutonic quench zones in the Kap Edvard Holm Layered Gabbro Complex, East Greenland: Journal of Petrology, v. 34, p. 681–710.

Wager, L. R., 1947, Geological investigations in East Greenland, Part IV: The stratigraphy and tectonics of Knud Rasmussens Land and the Kangerdlugssuaq region: Meddelelser om Grønland, v. 134, number 5.

Wager, L. R., and Brown, G. M., 1967, Layered igneous rocks: San Francisco, Freeman W. H. and Company, 588 p.

Wakita, H., Rey, P., and Schmitt, R. A., 1971, Abundances of the 14 rare-earth elements and 12 other trace elements in Apollo 12 samples: five igneous and one breccia rocks and four soils: Proceedings of the Second Lunar Science Conference, v. 2, p. 1319–1329.

Watson, E. B., 1982, Basalt contamination by continental crust: some experiments and models: Contributions to Mineralogy and Petrology, v. 80, p. 73–87.

Watson, E. B., and Baker, D. R., 1991, Chemical diffusion in magmas: an overview of experimental results and geochemical applications, *in* Perchuk, L. L., and Kushiro, I., editors, Physical chemistry of magmas: Berlin, Springer-Verlag, p. 120–151.

Watson, E. B., and Green, T. H., 1981, Apatite/liquid partition coefficients for the rare earth elements and strontium: Earth and Planetary Science Letters, v. 56, p. 405–421.
Watson, E. B., and Jurewicz, S. R., 1984, Behavior of alkalies during diffusive interaction of granitic xenoliths with basaltic magma: Journal of Geology, v. 92, p. 121–131.
Wilson, J. R., and Larsen, S. B., 1985, Two-dimensional study of a layered intrusion—the Hyllingen Series, Norway: Geological Magazine, v. 122, p. 97–124.
Yoder, H. S., and Tilley, C. E., 1962, Origin of basalt magmas; an experimental study of natural and synthetic rock systems: Journal of Petrology, v. 3, p. 342–532.